Global Biogeochemical Cycles®

RESEARCH ARTICLE
10.1029/2022GB007378

Special Section:
The U.S. GEOTRACES Pacific Meridional Transect (GP15)

^{210}Pb and ^{7}Be as Coupled Flux and Source Tracers for Aerosols in the Pacific Ocean

Ziran Wei[1], J. Kirk Cochran[1], Evan Horowitz[1], Patrick Fitzgerald[1], Christina Heilbrun[1], David Kadko[2], Mark Stephens[2], Chris M. Marsay[3], Clifton S. Buck[3], and William M. Landing[4]

[1]Stony Brook University, School of Marine and Atmospheric Sciences, Stony Brook, NY, USA, [2]Florida International University, Applied Research Center, Miami, FL, USA, [3]Skidaway Institute of Oceanography, University of Georgia, Savannah, GA, USA, [4]Department of Earth, Ocean and Atmospheric Science, Florida State University, Tallahassee, FL, USA

Abstract Deposition of aerosols to the surface ocean is an important factor affecting primary production in the surface ocean. However, the sources and fluxes of aerosols and associated trace elements remain poorly defined. Aerosol ^{210}Pb, ^{210}Po, and ^{7}Be data were collected on US GEOTRACES cruise GP15 (Pacific Meridional Transect, 152°W; 2018). ^{210}Pb fluxes are low close to the Alaskan margin, increase to a maximum at ~43°N, then decrease to lower values. There is good agreement between ^{210}Pb fluxes and long-term land-based fluxes during the SEAREX program (1970–1980s), as well as between GP15 and GP16 (East Pacific Zonal Transect, 12°S; 2013) at adjacent stations. A normalized fraction f(^{7}Be, ^{210}Pb) is used to discern aerosols with upper (high f) versus lower (low f) troposphere sources. Alaskan/North Pacific aerosols show significant continental influence while equatorial/South Pacific aerosols are supplied to the marine boundary layer from the upper troposphere. Lithogenic trace elements Al and Ti show inverse correlations with f(^{7}Be, ^{210}Pb), supporting a continental boundary layer provenance while anthropogenic Pb shows no clear relationship with f(^{7}Be, ^{210}Pb). All but four samples have ^{210}Po/^{210}Pb activity ratios <0.2 suggesting short aerosol residence time. Among the four samples (^{210}Po/^{210}Pb = 0.42–0.88), two suggest an upper troposphere source and longer aerosol residence time while the remaining two cannot be explained by long aerosol residence time nor a significant component of dust. We hypothesize that enrichments of ^{210}Po in them are linked to Po enrichments in the sea surface microlayer, possibly through Po speciation as a dissolved organic or dimethyl polonide species.

Key Points:

- North Pacific aerosols are influenced by continental sources while South Pacific aerosols have upper troposphere sources
- ^{7}Be/^{210}Pb shows that Al, Ti, and Fe have continental-influenced lower troposphere sources; Pb has lower- and upper troposphere sources
- Elevated aerosol ^{210}Po/^{210}Pb may indicate addition of Po from the sea surface as an organic Po or dimethyl polonide species

Supporting Information:

Supporting Information may be found in the online version of this article.

Correspondence to:

J. K. Cochran,
kirk.cochran@stonybrook.edu

Citation:

Wei, Z., Cochran, J. K., Horowitz, E., Fitzgerald, P., Heilbrun, C., Kadko, D., et al. (2022). ^{210}Pb and ^{7}Be as coupled flux and source tracers for aerosols in the Pacific Ocean. *Global Biogeochemical Cycles*, *36*, e2022GB007378. https://doi.org/10.1029/2022GB007378

Received 2 MAR 2022
Accepted 14 JUL 2022

Author Contributions:

Conceptualization: Ziran Wei, J. Kirk Cochran, David Kadko, Chris M. Marsay, Clifton S. Buck, William M. Landing
Data curation: Ziran Wei, J. Kirk Cochran, Evan Horowitz, Patrick Fitzgerald, Christina Heilbrun, Mark Stephens, Chris M. Marsay, Clifton S. Buck, William M. Landing
Formal analysis: Ziran Wei, J. Kirk Cochran, Chris M. Marsay, Clifton S. Buck, William M. Landing
Funding acquisition: Ziran Wei, J. Kirk Cochran, David Kadko, Chris M. Marsay, Clifton S. Buck, William M. Landing

1. Introduction

1.1. Overview

Deposition of aerosols to the surface ocean, particularly the open ocean away from continental land masses, is an important source of micronutrients, including trace metals such as Fe, Co, and Zn. The introduction of these and other elements to the surface ocean by atmospheric deposition may alleviate nutrient limitation and spur primary production. Iron limitation may impact ~30% of the surface ocean (Moore et al., 2013). This process links the biogeochemical cycling of trace elements with the global carbon cycle as well as the marine nitrogen cycle. Observations of aerosol concentrations over the open ocean remain limited due to the relatively short duration of research expeditions and the ephemeral nature of dust events that are responsible for most transport of mineral aerosols. However, aerosol deposition is the primary source of biolimiting trace elements to the surface ocean in many areas of the ocean, particularly the oligotrophic subtropical gyres (Pavia et al., 2020). Global models of the marine iron cycle have demonstrated that this process is poorly constrained, underscoring the need to improve estimates of aerosol deposition to the ocean (Tagliabue et al., 2016).

The chemical nature of these aerosols, and post deposition fate, is influenced by their sources and exposure to processing during atmospheric transport. For example, aerosol iron originating from combustion processes dissolves more readily than that which is derived from lithogenic sources. Aerosol source may be inferred from the ratio of elements contained within aerosol particles, for example, the relative abundance of a trace element to lithogenic tracers like Al or Ti, and transport pathways deduced from air mass back trajectory modeling (e.g., Marsay et al., 2022). Chemical analyses of aerosols require their capture onto filters by vacuum filtration from the atmosphere. This strategy produces a measure of aerosol loading or concentration in the air but does not provide a means to assess deposition flux directly. An estimate of aerosol deposition velocity is needed to convert

Investigation: Ziran Wei, J. Kirk Cochran, Evan Horowitz, Patrick Fitzgerald, Christina Heilbrun, David Kadko, Mark Stephens
Methodology: Ziran Wei, J. Kirk Cochran, Evan Horowitz, Patrick Fitzgerald, Christina Heilbrun, David Kadko, Mark Stephens, Chris M. Marsay, Clifton S. Buck, William M. Landing
Project Administration: Ziran Wei, J. Kirk Cochran, Chris M. Marsay
Resources: Ziran Wei, J. Kirk Cochran, David Kadko
Supervision: Ziran Wei, J. Kirk Cochran
Validation: Ziran Wei, J. Kirk Cochran, David Kadko
Visualization: Ziran Wei, J. Kirk Cochran
Writing – original draft: Ziran Wei, J. Kirk Cochran
Writing – review & editing: Ziran Wei, J. Kirk Cochran, Evan Horowitz, Patrick Fitzgerald, Christina Heilbrun, Mark Stephens, Chris M. Marsay, Clifton S. Buck, William M. Landing

concentration in the air to a flux from the atmosphere to the surface ocean. Thus, additional chemical tools are required to more fully understand the relevant processes.

The natural radionuclides ^{210}Pb (half-life = 22.3 years) and ^{7}Be (half-life = 53 days) are both produced in the atmosphere but have distinctly different sources that make them useful tracers of aerosols. ^{210}Pb is a member of the ^{238}U-decay series and, in the atmosphere, is produced from the decay of ^{222}Rn (half-life = 3.8 days) that has emanated from rocks and soils. ^{7}Be is a cosmogenic radionuclide produced as a result of cosmic ray spallation on target N and O atoms in the atmosphere. These different modes of production lead to different distributions of the two radionuclides in the atmosphere. ^{210}Pb production is principally in the lower troposphere owing to its land-based source, while ^{7}Be is dominantly produced in the upper troposphere and lower stratosphere. Production rates of both ^{210}Pb and ^{7}Be vary over the Earth's surface. For ^{210}Pb, the flux of ^{222}Rn from the oceans is only ∼2% of that from land areas (Wilkening & Clements, 1975).

The maximum concentration of ^{7}Be is found in the stratosphere at a height of 15–18 km (Lal & Peters, 1967), and its production decreases by ∼two orders of magnitude from the tropopause to the Earth's surface. In addition, because the cosmic ray flux is modulated by the Earth's magnetic field, ^{7}Be production increases from the equator toward the pole. Indeed, the production of ^{7}Be integrated over the atmospheric column increases by ∼5 to 7-fold from the equator to ∼60° and remains constant from 60 to 90° (Lal & Peters, 1967; Usoskin & Kovaltsov, 2008).

Both ^{210}Pb and ^{7}Be are particle reactive and are scavenged onto atmospheric aerosols. The fluxes of these radionuclides to the Earth's surface are mediated by scavenging of aerosols by wet and dry deposition, with wet deposition (i.e., rain, snow) generally dominating the removal from the atmosphere (Renfro et al., 2013 and references therein), except in very arid regions (Baskaran, 2011). The fluxes of ^{210}Pb or ^{7}Be (typically as dpm/cm^2/y) can be measured in several ways: direct collection of precipitation (Baskaran et al., 1993; Lozano et al., 2011; Peirson et al., 1966; Renfro et al., 2013; Turekian et al., 1983) or as the product of the aerosol deposition (or piston) velocity and the aerosol ^{210}Pb or ^{7}Be activity. For ^{210}Pb, inventories of ^{210}Pb excess in soil cores (Benninger et al., 1975; Dörr & Münnich, 1991; Graustein & Turekian, 1986; Monaghan, 1989; H. A. Moore & Poet, 1976) also have been used as a measure of the long-term flux.

Once scavenged by aerosols, ^{210}Pb decays to the intermediate daughter ^{210}Bi (half-life = 5 days) and then to ^{210}Po (half-life = 138.4 days). The relationships among the three radionuclides (i.e., the ^{210}Bi/^{210}Pb and ^{210}Po/^{210}Pb activity ratios) have been used as tracers of aerosol residence time (Lambert & Nezami, 1965; Papastefanou, 2006; Piliposian & Appleby, 2003; Rastogi & Sarin, 2008). Additional applications of ^{210}Pb and ^{210}Po include tracking the movement of air masses and studying the provenance of aerosols (Moriizumi et al., 1996; Obrist et al., 2006; Turekian et al., 1989). ^{210}Po is also produced from ^{210}Pb decay in the ocean and its biogeochemistry is distinct from that of ^{210}Pb. Po is a bioreactive element, incorporated into tissue possibly as an analog of sulfur. It also is cycled with organic matter and may undergo sea-air exchange in association with other biovolatile species such as dimethyl sulfide (Kim et al., 2000).

The distinctly different modes of introduction of ^{210}Pb and ^{7}Be to the atmosphere make them useful tracers of aerosol source. ^{7}Be is considered a more representative tracer for upper troposphere/lower stratosphere-sourced aerosols while ^{210}Pb is a useful tracer for continental boundary layer aerosols (Koch et al., 1996). As a consequence, the aerosol ^{7}Be/^{210}Pb activity ratio can be used to trace the region of the atmosphere where the radionuclides were scavenged by aerosol particles (Graustein & Turekian, 1996; Turekian & Graustein, 2003).

1.2. GEOTRACES Pacific Sampling (GP15 and GP16)

The international GEOTRACES program provides an ideal opportunity to study simultaneously the distributions of ^{210}Pb and ^{7}Be in aerosols at sea. Two cruises were conducted in the Pacific Ocean: The East Pacific Zonal Transect (GP16) along ∼12°S from October to December 2013 and the Pacific Meridional Transect (GP15) along 152°W from September to December 2018 (Figure 1). Aerosol samples from both cruises were analyzed for ^{7}Be (Buck et al., 2019, Kadko, Aguilar-Islas, et al., 2020; Kadko, Landing, & Buck., 2020) and ^{210}Pb (Niedermiller & Baskaran, 2019; this study). Both transects began near continents (South America for GP16 and North America for GP15) and moved to open ocean sites. The GP15 transect spanned several biogeochemical provinces, including the high primary production areas of the Alaskan Margin, North and Equatorial Pacific as well as oligotrophic regions associated with the subtropical gyres in both the North and South Pacific Ocean. The aerosols collected during these two transects have different source regions and transport paths through the atmosphere as well as

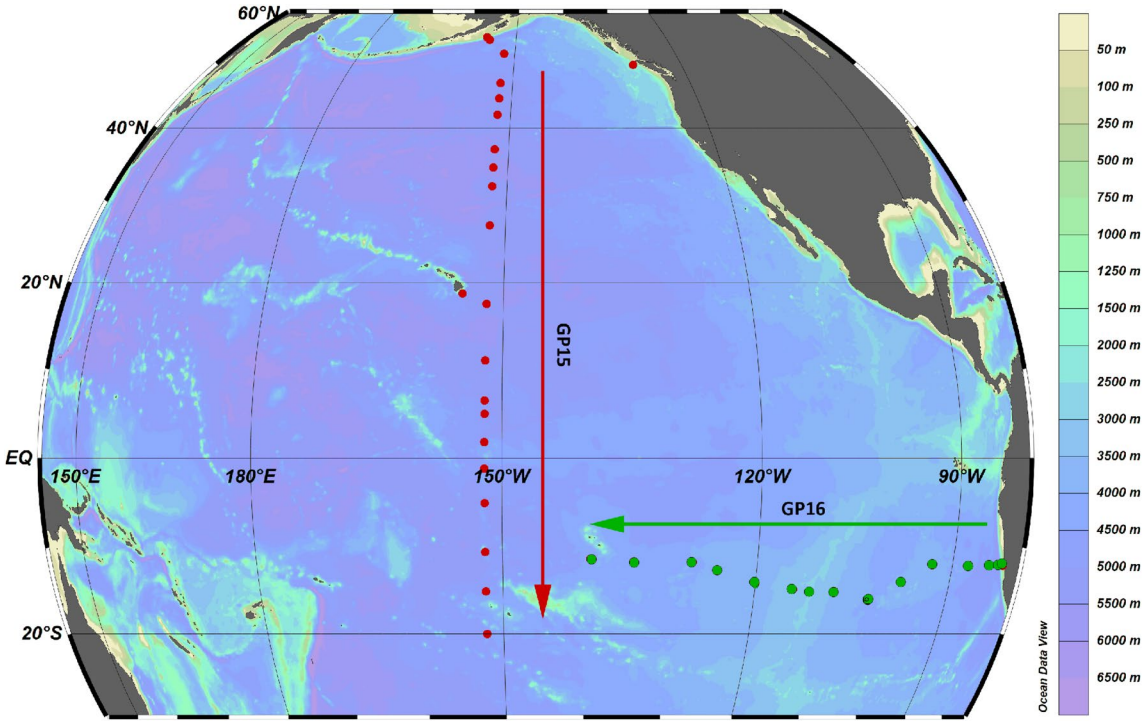

Figure 1. Aerosol sampling along the GEOTRACES GP15 (red) and GP16 (green) transects. Dots represent the midpoint of aerosol sample deployments. Arrows indicate direction of cruise/sampling. Color scale indicates water depth.

concentrations and deposition rates of significantly different magnitudes (Buck et al., 2019; Marsay et al., 2022). Here, we combine the aerosol ^{7}Be and ^{210}Pb data from both cruises to better determine aerosol fluxes and sources of the radionuclides as well as associated aerosol trace elements. This study also adds to the combined global aerosol data sets of ^{210}Pb (and ^{210}Po) and ^{7}Be (Zhang et al., 2021).

2. Methods

Bulk aerosol samples were collected throughout the cruise on 12-replicate acid-washed, 47-mm Whatman 41 (W41) ashless filter discs mounted in Advantec-MFS polypropylene open-face filter holders. Sampling details are further described in Buck et al. (2019) and Kadko, Landing, and Buck (2020). Three filters with combined filtered air volumes of ~360–1100 m^3 were provided for ^{210}Po and ^{210}Pb measurement.

The filters were placed in microwave digestion vessels, spiked with ^{209}Po tracer (1.76 dpm) and 10 mg stable Pb, and totally dissolved in a mixture of concentrated 5 mL of HCl, HNO_3, and HF. Sample solutions were centrifuged, evaporated to dryness, redissolved in concentrated HCl, evaporated again, and picked up in 1.5N HCl for plating. Po was plated onto silver discs with heating for 3 hr and the planchets were counted on Canberra passivated implanted planar silicon (PIPS) detectors coupled to a Mirion Alpha Analyst™ alpha spectrometer. Residual Po was removed from the initial plating solutions by suspending a piece of scrap Ag in them for 5 days, with periodic stirring, after which they were transferred to polycarbonate bottles for storage and ingrowth of additional ^{210}Po. Selected samples were plated again after the scrap Ag removal to determine residual Po left in the sample after this procedure; 5.0 ± 1.6% of the ^{209}Po initially added remained after the cleanup with scrap Ag.

An aliquot of each stored solution was analyzed for Pb concentration by Inductively Coupled-Plasma Mass Spectroscopy to determine Pb recoveries. Recoveries generally ranged from 83% to 100% (average 92 ± 6%). A second plating was carried out after ~6 months of storage to determine ^{210}Pb from ingrown ^{210}Po. All activities were corrected as appropriate to the time of sample collection, as described in Rigaud et al. (2013), and complete details are given in Wei (2021). ^{210}Pb activities were corrected for residual Po remaining after the scrap Ag cleanup step (see above). Detector backgrounds and blanks were subtracted from all samples. Backgrounds were typically low, averaging 0.00018 ± 0.00028 counts per minute (cpm) for ^{210}Po and 0.00039 ± 0.00021 cpm

Table 1
^{210}Pb and ^{210}Po Data for Aerosol Samples Collected Along the GEOTRACES Pacific Meridional Transect (GP15)

Cruise	GEOTRACES #	Aerosol Deployment #	Mid-point Latitude	Mid-point Longitude	Air volume (m^3)	^{210}Pb (dpm/100 m^3)	±	^{210}Po (dpm/100 m^3)	±	^{210}Po/^{210}Pb (dpm/dpm)	±
GP15	12318	Aer1	51.1	−132.16	357.0	0.48	0.02	−0.03	0.01	−0.06	0.02
GP15	12699	Aer3	54.9	−155.45	503.4	0.12	0.02	0.05	0.04	0.42	0.34
GP15	12813	Aer4	53.3	−153.59	1089.0	0.35	0.02	−0.05	0.05	−0.14	0.14
GP15	12947	Aer5	49.5	−152	814.5	1.60	0.07	0.34	0.23	0.21	0.14
GP15	13072	Aer6	45.75	−152	550.2	1.94	0.09	−0.07	0.26	−0.04	0.13
GP15	13182	Aer7	43.25	−152	558.6	2.52	0.12	−0.19	0.32	−0.08	0.13
GP15	13288	Aer8	39.5	−152	799.8	0.56	0.06	0.49	0.17	0.88	0.32
GP15	13388	Aer9	35.75	−152	677.1	1.3	0.06	0.10	0.16	0.08	0.12
GP15	13532	Aer10	33.25	−152	842.4	0.82	0.04	−0.02	0.10	−0.03	0.12
GP15	13716	Aer11	29.5	−152	747.6	0.51	0.02	0.34	0.10	0.67	0.20
GP15	13866	Aer12	24.5	−152	620.4	0.67	0.03	0.03	0.09	0.04	0.13
GP15	14047	Aer13	18.1	−153.45	532.2	0.50	0.02	0.00	0.07	0.00	0.14
GP15	14225	Aer14	14.25	−152	744.0	0.54	0.03	−0.01	0.07	−0.02	0.13
GP15	14502	Aer15	8.8	−152	733.2	0.17	0.01	0.00	0.03	−0.02	0.18
GP15	14633	Aer16	5.725	−152	681.0	0.46	0.02	−0.08	0.06	−0.17	0.13
GP15	14782	Aer17	3.45	−152	797.4	0.40	0.02	0.03	0.06	0.08	0.15
GP15	14962	Aer18	0.415	−152	887.7	0.73	0.04	−0.06	0.11	−0.08	0.15
GP15	15155	Aer19	−3.1	−152	703.2	0.60	0.03	0.02	0.09	0.03	0.15
GP15	15316	Aer20	−7.75	−152	815.1	0.38	0.02	0.00	0.06	−0.01	0.16
GP15	15652	Aer21	−12.75	−152	793.2	0.17	0.01	0.12	0.03	0.68	0.18
GP15	15810	Aer22	−17.5	−152	935.1	0.32	0.02	0.01	0.04	0.03	0.12
GP15	15852	Aer23	−19.6	−151.62	459.3	0.40	0.02	−0.07	0.05	−0.18	0.13

for ^{209}Po. Blank activities were 0.0023 ± 0.0016 dpm for ^{210}Po and 0.053 ± 0.006 for ^{210}Pb and were <0.5% of the measured ^{210}Po activities and <5% of ^{210}Pb activities. Errors were propagated using standard error propagation formulas (Rigaud et al., 2013) and included counting errors on sample, background, and blank ^{210}Po and ^{209}Po, spiking errors, and uncertainty of the ^{209}Po tracer activity.

3. Results and Discussion

3.1. ^{210}Po and ^{210}Pb Activities and Activity Ratios

The ^{210}Pb and ^{210}Po data from the GP15 transect are given in Tables 1 and 2. ^{210}Pb activities range from 0.12 to 2.52 disintegrations per minute per 100 m^3 (dpm/100 m^3). The Aer1 sample was collected at ∼51°N, 132°W, before the 152°W transect sampling began. Along the 152°W transect (samples Aer3 to Aer23), the ^{210}Pb activity increases from 0.12 dpm/100 m^3 at ∼55°N to a maximum between 42°N and 52°N and peaking at 2.5 dpm/100 m^3 (∼43°N; Aer7), after which it decreases to values generally less than 1.0 dpm/100 m^3 (Figures 2 and 3). Table 3 includes the published ^{210}Pb data from the GEOTRACES East Pacific zonal transect (GP16; Niedermiller & Baskaran, 2019). A similar trend of decreasing activities away from the continent (South America) is observed (Figure 3). The zonal transect (GP16) ended at 142.95°W (−11.03°S), where the ^{210}Pb activity was 0.51 ± 0.02 dpm/100 m^3. In comparison, two deployments during GP15 collected near that region (7.75°S and 12.75°S; Aer20 and Aer21, respectively) have ^{210}Pb activities of 0.38 ± 0.02 and 0.17 ± 0.01 dpm/100 m^3, respectively.

The samples collected during GP15 were measured for ^{7}Be using gamma spectrometry (Kadko, Landing, & Buck, 2020) before they were processed for ^{210}Po and ^{210}Pb. This resulted in a longer than usual delay, ∼5 months,

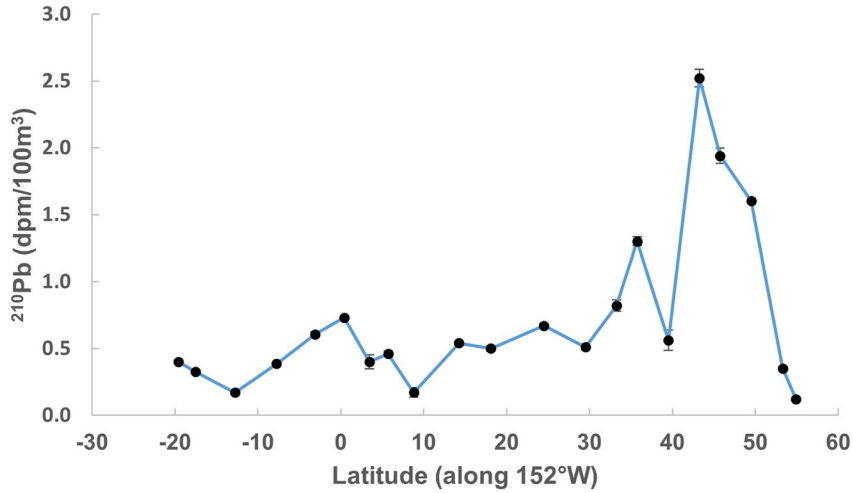

Figure 2. Aerosol ^{210}Pb activities (dpm/100 m^3) along the GP15 (152°W) transect. Propagated error bars are plotted but may be smaller than the size of the symbols. Positive latitudes are north.

in processing samples for initial ^{210}Po. Aerosol samples typically have ^{210}Po << ^{210}Pb (^{210}Po/^{210}Pb activity ratio <0.2; Baskaran, 2011), and thus most of the initial ^{210}Po measured was produced by ^{210}Pb decay in the sample since collection. Subtracting the blank and ingrown ^{210}Po from the measured ^{210}Po produced low ^{210}Po and ^{210}Po/^{210}Pb values with large errors clustering around zero (Table 1; Figure 4). We report all these values in Table 1, including the negative ones, because they indicate that initial ^{210}Po activities were low for most of the samples. Exceptions were evident for deployments centered around 54.9°N (Aer3), 49.5°N (Aer5), 39.5°N (Aer8), 29.5°N (Aer11), and 12.75°S (Aer21) (Table 1). The highest ratio was found at 39.5°N with a value of 0.88 ± 0.32. These samples are discussed in more detail in Section 3.4.

Activities of ^{7}Be were measured on all aerosol samples from both GP15 and GP16 and the data have been published (Buck et al., 2019; Kadko, Aguilar-Islas, et al., 2020; Kadko, Landing, & Buck, 2020). We include them in Tables 2 and 3 because we will use the ^{7}Be/^{210}Pb ratio as an aerosol source tracer.

3.2. Atmospheric ^{210}Pb Fluxes

Here, we determine ^{210}Pb fluxes as the product of the bulk deposition velocity (i.e., transport due to both wet and dry deposition) determined from ^{7}Be and the aerosol ^{210}Pb activity. Beryllium is a particle-reactive element and can be scavenged from seawater, for example, in the coastal ocean. However, earlier work (Bloom & Crecelius, 1983; Merrill et al., 1960; Silker, 1972; Silker et al., 1968) found that particulate ^{7}Be activities in the open ocean are typically <10% of the total ^{7}Be inventory (Silker, 1972; Kadko & Prospero, 2011). Indeed, Kadko and Prospero (2011) found good agreement between the independently measured atmospheric flux of ^{7}Be and water column inventories. Coupled with undetectable particulate activities (Andrews et al., 2008), these results suggest that the rate of scavenging of ^{7}Be is negligible in the open ocean relative to its half-life (53 days) and makes possible its use as a quasi-conservative tracer of ocean mixing rates in the upper water column.

Young and Silker (1980) proposed that measuring the profile of ^{7}Be in the upper ocean and determining its inventory (dpm/m^2) could be used to calculate its flux from the atmosphere (dpm/m^2/y) as aerosols are scavenged by wet and dry deposition, as noted above. Simultaneous measurement of the aerosol activity of ^{7}Be (dpm/m^3) provides a means of determining the deposition velocity of aerosols that supply ^{7}Be (and presumably ^{210}Pb and trace elements) to the ocean surface (Young & Silker, 1980):

$$V_b = \frac{F_{^7Be}}{[^7Be]} \quad (1)$$

where V_b is the bulk deposition velocity (m/y), $F_{^7Be}$ is the ^{7}Be atmospheric flux (dpm/m^2/y), and [^{7}Be] is the aerosol ^{7}Be concentration (dpm/m^3). Equation 1 assumes steady state for the ^{7}Be flux and thus its inventory in the upper water column Kadko and Olson (1996); Kadko and Prospero (2011); Young and Silker (1980).

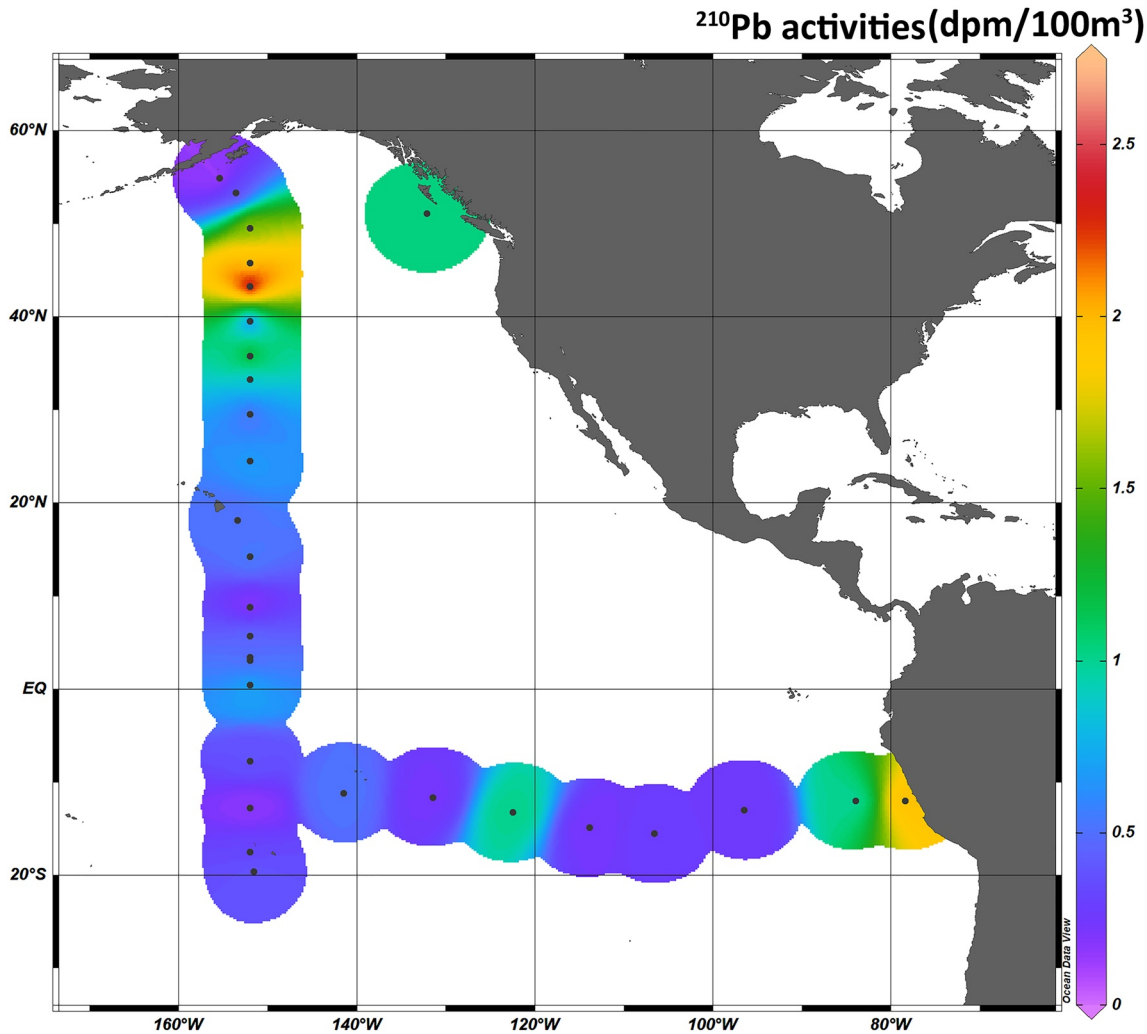

Figure 3. Compilation of aerosol ^{210}Pb activities (dpm/100 m^3) along both the GP15 (152°W) and GP16 (12°S) transects; Data for GP16 are from Niedermiller and Baskaran (2019).

Kadko and Prospero (2011) found that temporal variation of the ^{7}Be flux determined from the ocean inventories near Bermuda was within ~25% (480 ± 100 dpm/m^2/d) and was comparable to the flux determined by direct collection of precipitation (480 ± 270 dpm/m^2/d).They also observed that only 5% of the ^{7}Be inventory could be supplied by dry deposition, reinforcing that most ^{7}Be (and implicitly ^{210}Pb) is delivered to the ocean surface via wet deposition.

The deposition velocities based on ^{7}Be were calculated and reported by Kadko, Landing, and Buck (2020) for GP15 and Buck et al. (2019) for GP16. For GP16, the method described above was used at each station (Buck et al., 2019). In the case of GP15, upwelling of ^{7}Be-deficient water at the equator alters the ^{7}Be inventory so that it does not reflect the atmospheric deposition. As a consequence, Kadko, Landing, and Buck (2020) developed a relationship between deposition velocity and climatic average rainfall that facilitated determination of the deposition velocity in the upwelling region near the equator. Rainfall data were obtained from the Global Precipitation Climatology Project and used to calculate the relationship between rainfall and V_b for GP15 (Kadko, Landing, & Buck, 2020). The deposition velocity values used are summarized in Tables 2 and 3. Values on GP15 average 2.7 ± 1.5 cm/s (2330 ± 1300 m/d) and 1.8 ± 0.7 cm/s (1560 ± 600 m/d) on GP16. These are within the range of deposition velocities reported for ^{210}Pb (0.1–5.0 cm/s), derived in a similar fashion (Baskaran, 2011). In oceanic settings, for example, Turekian and Cochran (1981a, 1981b) reported values of 0.25 cm/s and 1.0 cm/s for

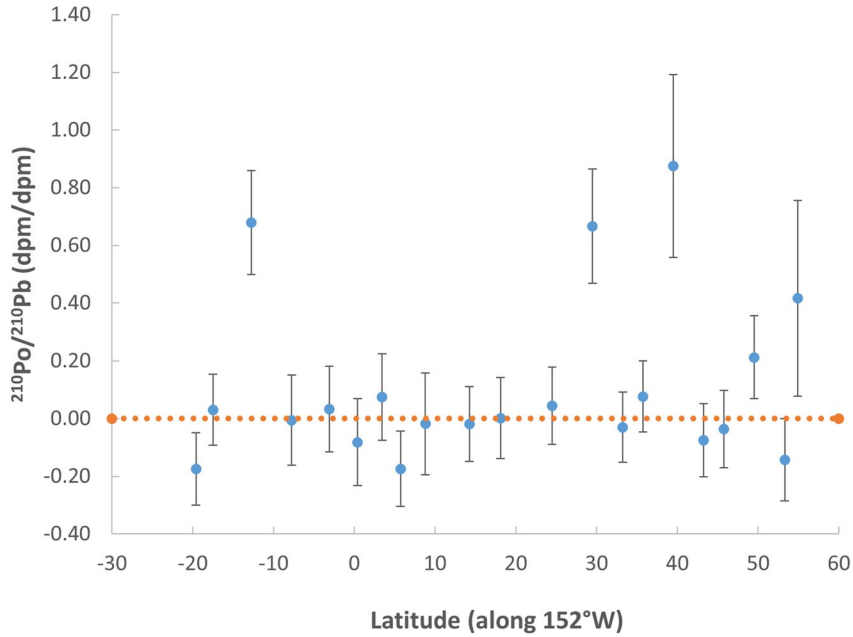

Figure 4. Initial ^{210}Po/^{210}Pb activity ratios in aerosols along the GP15 (152°W) transect. Positive latitudes are north. Orange dotted line corresponds to ^{210}Po/^{210}Pb activity ratio of 0. Most values scatter about the line indicating low initial activity ratios. Ingrowth and decay corrections for initial ^{210}Po were large due to the long time interval between sampling sand initial ^{210}Po plating. See text for discussion.

Enewetak during the dry and wet seasons, respectively, and ~3 cm/s for Hawaii. Turekian et al. (1983) measured 1.0 cm/s during the summer season in Bermuda.

The atmospheric flux of ^{210}Pb (F_{210Pb}) is calculated from the bulk deposition velocity as

$$F_{210Pb} = V_b \times [^{210}Pb]atm \quad (2)$$

where $[^{210}Pb]atm$ is the aerosol activity of ^{210}Pb. ^{210}Pb fluxes calculated using Equation 2 are given in Tables 2 and 3. For GP16 (Table 3), we recalculated the ^{210}Pb flux using the ^{7}Be-derived deposition velocities for each sample (Buck et al., 2019). The ^{210}Pb fluxes reported by Niedermiller and Baskaran (2019) are included in Table 3 for comparison. The latter fluxes assumed a constant deposition velocity of 1 cm/s (864 m/d). The recalculated ^{210}Pb fluxes are somewhat larger than those of Niedermiller and Baskaran (2019) because the ^{7}Be-derived deposition velocities are generally >864 m/d. In the discussion that follows, we use the recalculated GP16 values to compare with the GP15 results.

The ^{210}Pb flux reflects the cumulative production from ^{222}Rn and scavenging as an air mass moves over the continent and the ocean. For example, Turekian et al. (1989) showed that the ^{210}Pb flux in the North Pacific as a function of longitude decreased markedly from values over Japan (~2 dpm/cm^2/y) to ~0.5 dpm/cm^2/y within 1000 km of the continent, decreasing further to ~0.2–0.3 dpm/cm^2/y by 6,000 km, and remaining constant across the eastern North Pacific. They attributed this pattern to rapid scavenging of continent-derived ^{210}Pb in the marine boundary layer as the air mass moved over the Pacific. The ^{210}Pb flux over the open North Pacific was then controlled by exchange of aerosols between the upper troposphere and marine boundary layer.

The ^{210}Pb flux varies with latitude along the GP15 section (Figure 5). Although the Alaskan margin is close to the North American continent, it has the lowest ^{210}Pb flux of the transect, with an average of 0.18 dpm/cm^2/y. Five-day air mass back trajectories show that the air sampled during deployments Aer3 and Aer4 had circulated over the Gulf of Alaska in the days prior to sampling (Marsay et al., 2021). In contrast, the back trajectories calculated for the Aer5-7 deployments farther south indicate transport from Russia in the 5–10 days prior to sample collection, and the ^{210}Pb fluxes are higher. The maximum ^{210}Pb flux is 1.69 dpm/cm^2/y as measured in Aer7 at 43°N. This partly reflects the air movements as the aerosol becomes dominated by the westerlies originating from Asia (Tsunogai et al., 1985). Such a trend is echoed by trace element data (e.g., Al, Ti), which will be explored

Table 2
^{210}Pb Fluxes and the Normalized ^{7}Be/^{210}Pb Fraction-f(^{7}Be, ^{210}Pb)- for Stations Along the GEOTRACES Pacific Meridional Transect (GP15)

GEOTRACES #	Aerosol ID #	V_b[a] (m/d)	^{210}Pb (dpm/m^3)	±	^{7}Be[b] (dpm/m^3)	±	f(^{7}Be, ^{210}Pb)[c]	±	^{210}Pb flux (dpm/cm^2/y)	±
12318	Aer1	2040	0.0048	0.0002	0.0622	0.0094	0.49	0.01	0.36	0.01
12699	Aer3	2140	0.0012	0.0002	0.0184	0.0066	0.54	0.22	0.09	0.01
12813	Aer4	2040	0.0035	0.0002	0.0366	0.0015	0.44	0.02	0.26	0.01
12947	Aer5	2340	0.016	0.0007	0.1567	0.0054	0.43	0.02	1.37	0.06
13072	Aer6	2240	0.0194	0.0008	0.266	0.0079	0.51	0.02	1.59	0.07
13182	Aer7	1840	0.0252	0.0011	0.2935	0.0089	0.47	0.02	1.69	0.08
13288	Aer8	1640	0.0056	0.0006	0.1232	0.0053	0.62	0.04	0.34	0.03
13388	Aer9	1940	0.013	0.0006	0.2730	0.0076	0.61	0.02	0.92	0.04
13532	Aer10	1610	0.0082	0.0004	0.1818	0.0073	0.63	0.03	0.48	0.02
13716	Aer11	1540	0.0051	0.0002	0.2770	0.0083	0.80	0.03	0.29	0.01
13866	Aer12	1740	0.0067	0.0003	0.1754	0.0075	0.66	0.04	0.43	0.02
14047	Aer13	1540	0.0050	0.0002	0.0975	0.0106	0.60	0.08	0.28	0.01
14225	Aer14	3840	0.0054	0.0003	0.0792	0.0084	0.53	0.06	0.76	0.04
14502	Aer15	5240	0.0017	0.0001	0.0413	0.0046	0.65	0.09	0.33	0.02
14633	Aer16	6340	0.0046	0.0002	0.0984	0.0059	0.62	0.05	1.06	0.05
14782	Aer17	1840	0.0040	0.0002	0.1848	0.0079	0.78	0.043	0.27	0.01
14962	Aer18	1240	0.0073	0.0004	0.1373	0.0053	0.59	0.03	0.33	0.02
15155	Aer19	1190	0.0061	0.0003	0.1222	0.0105	0.60	0.06	0.26	0.01
15316	Aer20	1640	0.0038	0.0002	0.1492	0.0074	0.75	0.05	0.23	0.01
15652	Aer21	1740	0.0017	0.0001	0.1080	0.0076	0.83	0.08	0.11	0.01
15810	Aer22	2140	0.0032	0.0002	0.1482	0.0066	0.78	0.04	0.25	0.01
15852	Aer23	2440	0.0040	0.0002	0.2147	0.0133	0.80	0.06	0.36	0.02

[a]Calculated using rainfall versus V_b relationship in Kadko, Landing, and Buck (2020). [b]Data from Kadko, Landing, and Buck (2020). [c]Normalized fraction of ^{7}Be/^{210}Pb-see text.

Table 3
^{210}Pb Fluxes and the Normalized ^{7}Be/^{210}Pb Fraction-f(^{7}Be, ^{210}Pb)- for the GEOTRACES East Pacific Zonal Transect (GP16)

GEOTRACES #	Aerosol ID #	Mid-point Latitude[a]	Mid-point Longitude[a]	V_b[b] (m/d)	^{210}Pb[d] (dpm/m^3)	±	^{7}Be[b] (dpm/m^3)	±	f(^{7}Be, ^{210}Pb)	±	^{210}Pb flux[c] (dpm/cm^2/y)	±	^{210}Pb flux[a] (dpm/cm^2/y)	±
2322	Aer2	−12.03	−78.43	835	0.0197	0.0007	0.305	0.024	0.58	0.05	0.60	0.02	0.620	0.020
3293	Aer4	−12.00	−84	1526	0.0099	0.0004	0.167	0.024	0.60	0.10	0.55	0.02	0.310	0.012
3768	Aer6	−13.00	−96.50	2076	0.0026	0.0001	0.123	0.025	0.81	0.21	0.20	0.01	0.082	0.003
8358	Aer8	−15.50	−106.60	2489	0.0029	0.0001	0.102	0.028	0.76	0.26	0.26	0.01	0.090	0.004
8821	Aer10	−14.88	−113.87	1330	0.0023	0.0001	0.113	0.020	0.82	0.19	0.11	0.00	0.073	0.003
9263	Aer12	−13.27	−122.50	1028	0.0102	0.0004	0.164	0.042	0.59	0.18	0.38	0.02	0.323	0.012
9718	Aer14	−11.64	−131.50	2127	0.0024	0.0001	0.089	0.030	0.77	0.33	0.19	0.01	0.076	0.003
10082	Aer16	−11.17	−141.48	1186	0.0051	0.0002	0.163	0.017	0.74	0.09	0.22	0.01	0.162	0.007

[a]Negative latitudes are south; negative longitudes are west. [b]From Buck et al. (2019). [c]Recalculated using V_b from Buck et al. (2019) and ^{210}Pb activity from Niedermiller and Baskaran (2019). [d]From Niedermiller and Baskaran (2019).

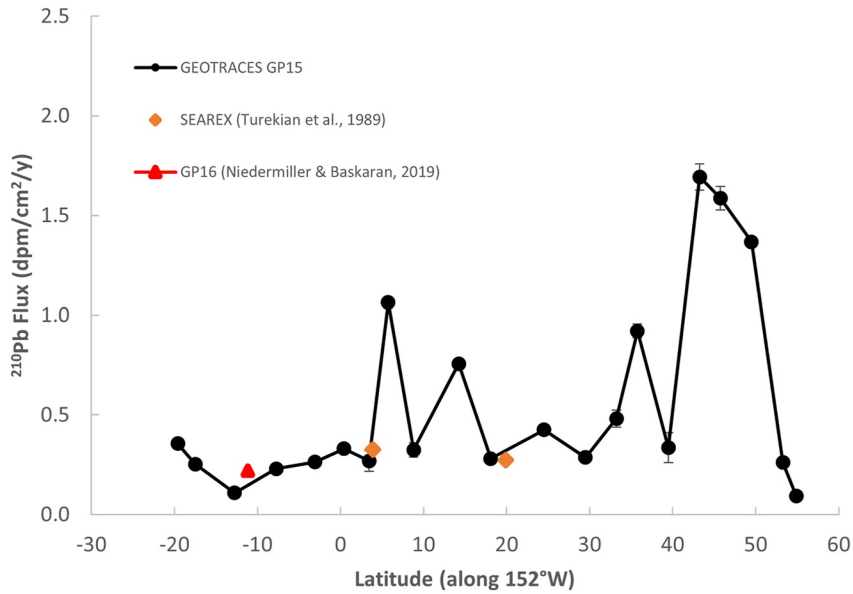

Figure 5. ^{210}Pb fluxes along the GP15 transect. Solid diamonds represent prior measurements of flux through annual collection of wet deposition at Fanning Island (~4°N) and Oahu (~20°N) (Turekian et al., 1989). The solid triangle is based on the aerosol ^{210}Pb value from the closest sample of the GP16 transect (Niedermiller & Baskaran, 2019), recalculated in the present study using the deposition velocity derived from ^{7}Be (Table 3). Positive latitudes are north.

in more detail below. The strength of the westerlies wanes in the tropical Pacific and remoteness from the continental land mass causes the ^{210}Pb fluxes to decrease progressively in the tropical and equatorial/South Pacific, where values are consistently less than 1 dpm/cm^2/y. This agrees with previous values for the North Pacific (Tsunogai et al., 1985; Turekian et al., 1989). Indeed, the ^{210}Pb fluxes determined from the GP15 sampling at Aer13 and Aer17 agree well with the previously determined values at Oahu (21°N 157°W) and Fanning Island (4°N 159°W), respectively (Figure 5). The latter were determined through direct collection of precipitation over approximately 1 year as part of the SEAREX program (Turekian et al., 1989). At Oahu, ^{210}Pb fluxes also were determined through the inventories of ^{210}Pb in soil profiles (Turekian et al., 1989), and the results were in good agreement, as seen in other comparisons of ^{210}Pb fluxes determined through direct collection of precipitation and inventories in soil profiles. The general agreement between these prior measurements of direct ^{210}Pb deposition and the ^{210}Pb fluxes calculated from the short-term aerosol collection during GP15 is encouraging and suggests that multiyear variation in flux is within ~20%, as indicated by land-based studies of ^{210}Pb flux (Renfro et al., 2013 and references therein).

The recalculated GP16 ^{210}Pb fluxes are also consistent with previous flux measurements in the Pacific (Niedermiller & Baskaran, 2019; Tsunogai et al., 1985; Turekian et al., 1989) and are largely consistent with the values given by Niedermiller and Baskaran (2019) using an assumed value of V_b. The GP15 and GP16 transects approach one another at ~12°S and the fluxes determined from Aer20 and Aer21 (centered around 7.75°S and 12.75°S, respectively) during GP15, bracket the value from the sample centered at 11.17°S during GP16 (Figure 6). These agreements generally confirm the long-term constancy of the ^{210}Pb flux, which as noted above, is largely considered to be insensitive (±20%) to annual variations at a given site (Baskaran, 2011; Turekian et al., 1977). For the GP16 transect, the highest ^{210}Pb flux is 0.6 dpm/cm^2/y, found in the coastal station that is heavily influenced by continental-derived ^{210}Pb (Figure 6). This contribution of continental aerosol will be explored further below (Section 3.3.2) using the ^{7}Be/^{210}Pb ratio.

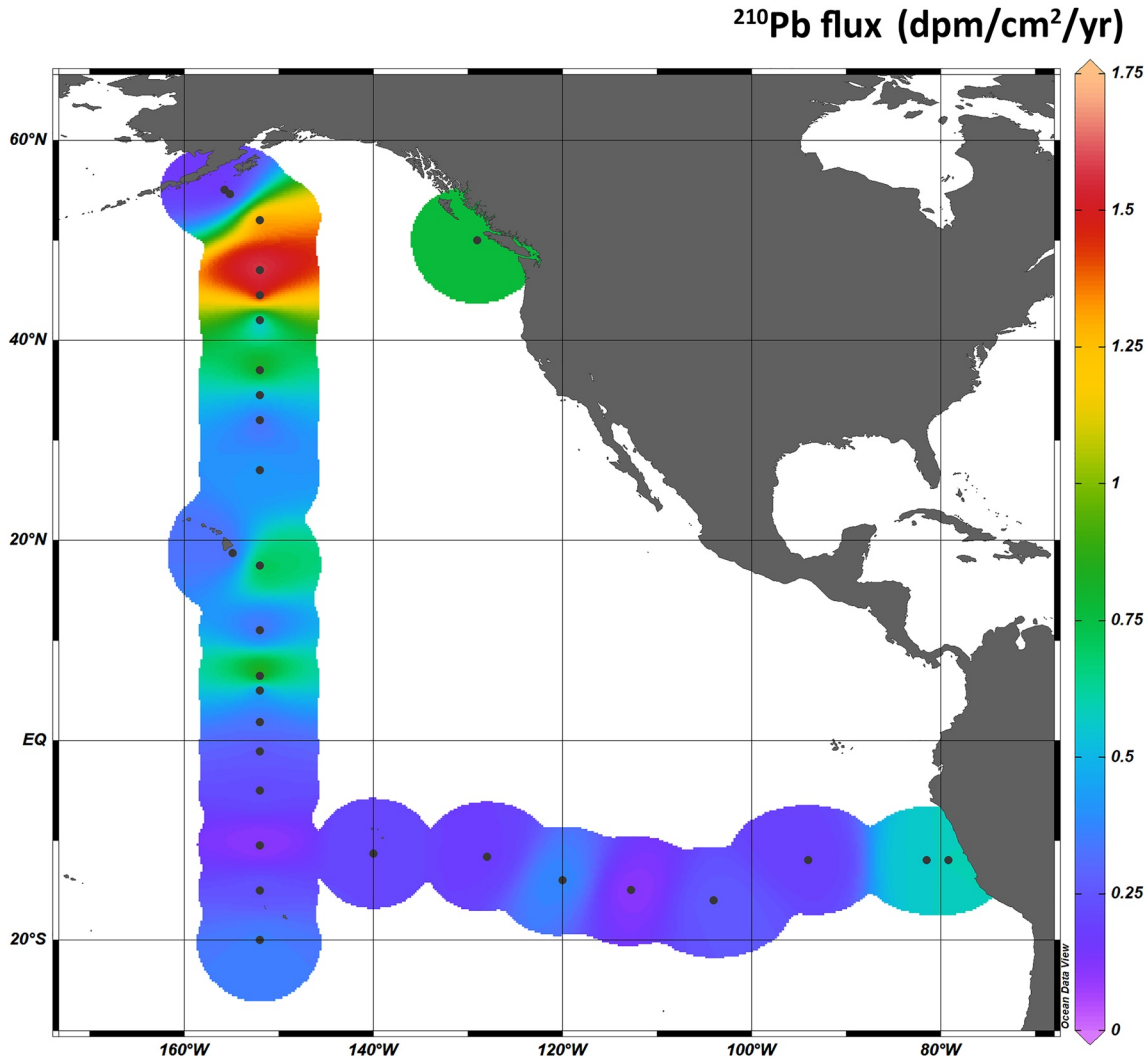

Figure 6. ^{210}Pb fluxes along GP15 and GP16 transects. GP16 fluxes have been recalculated from Niedermiller and Baskaran (2019); see Table 3 and text for discussion.

3.3. Application of the ^{7}Be/^{210}Pb Ratio as an Aerosol Source Tracer-the Normalized Fraction, f(^{7}Be, ^{210}Pb)

3.3.1. Definition and Calculation

In the application of ^{7}Be and ^{210}Pb as aerosol source tracers, Graustein and Turekian (1996) proposed the use of a "normalized fraction of ^{7}Be with respect to ^{210}Pb in a given sample" rather than the ^{7}Be/^{210}Pb activity ratio. They denoted the normalized fraction as f(^{7}Be, ^{210}Pb), defined as

$$f(^{7}\mathrm{Be},\ ^{210}\mathrm{Pb}) = \frac{^{7}Be}{^{7}Be + n^{210}Pb} \tag{3}$$

where n is approximated by the ratio of the standard deviation of ^{7}Be in a given set of samples to that of ^{210}Pb. A full derivation of f(^{7}Be, ^{210}Pb) is given in Graustein and Turekian (1996). The parameter is independent of precipitation scavenging and is a linear function of mixing in a two-component system. Graustein and Turekian (1996) argued that high values of f(^{7}Be, ^{210}Pb) correspond to upper atmosphere aerosol sources while low values represent continental boundary sources The values of f(^{7}Be, ^{210}Pb) can approach unity as an upper limit for stratospherically sourced aerosols and range to low values for those sourced in the lower troposphere boundary layer.

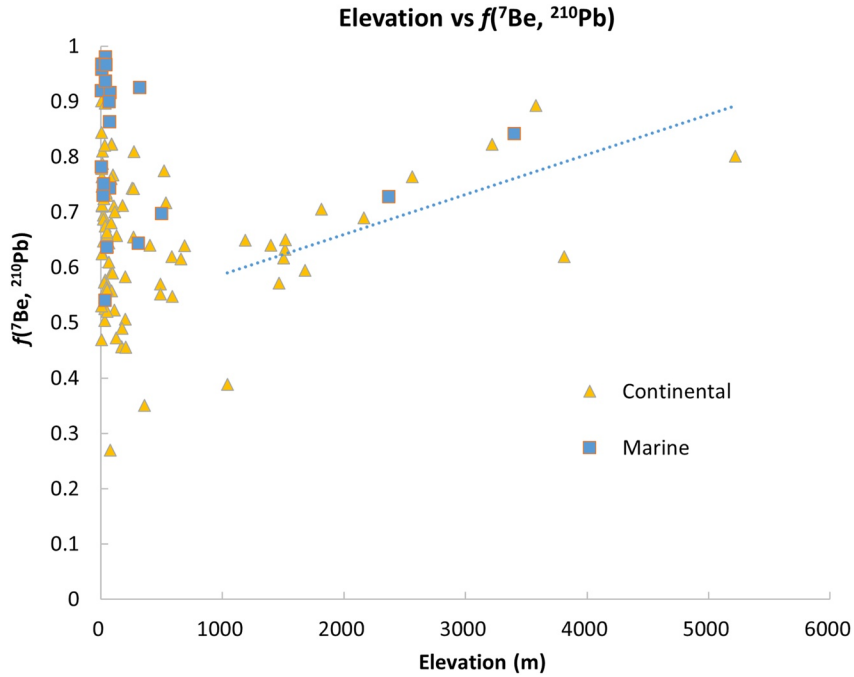

Figure 7. Normalized ratio $f(^{7}Be, ^{210}Pb)$ calculated from Zhang et al. (2021) and plotted as a function of elevation of sampling site. Only data with known altitudes are plotted. Only stations above 1000 m are selected for linear regression ($R^2 = 0.478$).

Graustein and Turekian (1996) applied the normalized fraction to determine sources of ozone to an ocean island setting. However, despite the usefulness of this parameter, only a handful of studies have subsequently made use of it (Lozano et al., 2011). Nevertheless, there are numerous studies that report both ^{7}Be and ^{210}Pb data, and Zhang et al. (2021) recently compiled these into a single database. Zhang et al. (2021) gave site information as well, and we have calculated the $f(^{7}Be, ^{210}Pb)$ values for each site using the standard deviations of ^{7}Be and ^{210}Pb for the entire data set. We separated the values by location into "marine," that is, oceanic and coastal sites, and "continental," that is, land-based but noncoastal sites. Sites were also grouped according to altitude (elevation) and the resultant values of $f(^{7}Be, ^{210}Pb)$ are plotted in Figure 7.

The values of $f(^{7}Be, ^{210}Pb)$ increase linearly with altitude above 1000m, as expected, because cosmogenic ^{7}Be dominates the aerosols collected in the upper atmosphere. A linear trend is observed for these high-altitude sites, despite the clear dearth of data above 1000m, compared with sites that are <1000m. Low-altitude aerosols display a range of $f(^{7}Be, ^{210}Pb)$ values, varying between 0.27 and 0.98. This is similar to the range observed by Graustein and Turekian (1996), ~0.2 to ~0.9, at their site in the Canary Islands.

For altitudes below 1000m, aerosols from continental and marine sites have means (±1SD) of 0.63 ± 0.13 and 0.85 ± 0.12, respectively. Such a difference is expected because marine aerosols far from land can be interpreted as dominated by upper atmosphere influences compared with continental aerosols. Some of the spread in the marine and continental data may be due to differences in ^{7}Be production as a function of latitude (Lal & Peters, 1967; Usoskin & Kovaltsov, 2008). We tested this possibility using the data compilation of Zhang et al. (2021). Across latitudes, no systematic variability is seen in aerosol ^{7}Be (Figures S1 and S2 in Supporting Information S1) at either marine or coastal sites, implying that latitudinal differences in ^{7}Be production (Usoskin & Kovaltsov, 2008) are not reflected in aerosol ^{7}Be measurements at the Earth's surface, possibly due to atmospheric mixing.

Temporal differences in ^{7}Be production caused by solar variability also could affect ^{7}Be production. This variability could be a factor when comparing the GP15 and GP16 data because the transects were carried out five years apart (2013 for GP16 and 2018 for GP15) and solar production (as indicated by sunspot number) was ~4 times higher in 2013 than in 2018 (https://wwwbis.sidc.be/silso/monthlyssnplot). Terzi et al. (2020) examined the relationship between annual average ground-level ^{7}Be in aerosols measured from 2004 to 2018 at 62 stations

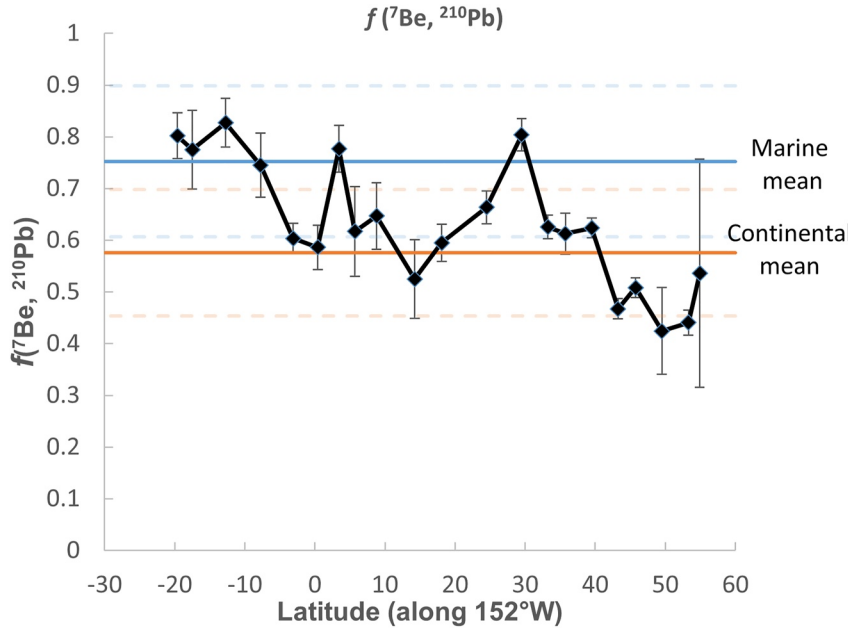

Figure 8. $f(^{7}Be, ^{210}Pb)$ along the GP15 transect. Horizontal lines represent the mean (solid) ± one standard deviation (dashed) calculated from all stations, from the compilation of Zhang et al. (2021) grouped into Marine (open ocean and coastal sites) and Continental (continental interior sites). Positive latitudes are north. See text for discussion.

worldwide as part of the International Monitoring System. In comparison with cosmic ray flux (inversely related to solar activity) over the same period, only 18 of the stations displayed a significant positive correlation. They concluded that at most stations any relationship was obscured by atmospheric processes and air-mass mixing. Consequently, we do not consider it further in interpreting the GP15 versus GP16 $f(^{7}Be, ^{210}Pb)$ data.

We also tested for latitudinal dependence of $f(^{7}Be, ^{210}Pb)$ that might be caused by latitudinal variation in ^{7}Be production. For the continental sites, no significant variation is seen with latitude, consistent with the ^{7}Be aerosol data cited above and the dominance of ^{210}Pb flux from continental land masses (Figure S4 in Supporting Information S1). In contrast, the marine sites do show a dependence, with higher values at high southern latitudes (Figure S3 in Supporting Information S1). However, these sites are farthest from continental land masses (and hence a source of ^{210}Pb), and we hypothesize that differences in $f(^{7}Be, ^{210}Pb)$ at marine sites provide a context for understanding the provenance of aerosols. We extend this approach to the aerosol $f(^{7}Be, ^{210}Pb)$ results from samples collected on GP15 and GP16.

3.3.2. Application of $f(^{7}Be, ^{210}Pb)$ to GEOTRACES GP15 and GP16

Values of $f(^{7}Be, ^{210}Pb)$ in aerosols collected on GP15 range between 0.43 and 0.83 (Figures 8 and 9; Table 2). Low values are found near the Alaskan Margin and the high latitudes of the Northern Pacific while high values are evident in the Equatorial/South Pacific region. Indeed, the southernmost four samples all have $f(^{7}Be, ^{210}Pb)$ values greater than or approximately equal to the mean of all marine sites worldwide, while only two samples exceed the marine mean among the remaining samples. Comparison of the pattern of ^{210}Pb fluxes along the GP15 transect with that of the $f(^{7}Be, ^{210}Pb)$ values shows an inverse relationship, such that regions with higher ^{210}Pb flux (Figure 6) have lower $f(^{7}Be, ^{210}Pb)$ (Figure 9). Aerosols in the northern part of the transect are dominated by lower troposphere sources while the marine boundary layer in the southern part of the transect is supplied by aerosols from the upper troposphere. This conclusion is similar to that of Turekian et al. (1977, 1989) based on the variation of ^{210}Pb fluxes away from the Asian landmass in the North Pacific. We observe the lowest values of $f(^{7}Be, ^{210}Pb)$ on the GP15 transect for the samples collected in closest proximity to continental landmasses, which is consistent with the prediction that aerosols there are dominated by continental sources. This is also true for two samples from the easternmost deployments during GP16 (Figure 9). Indeed, Figure 9 shows similar trends in $f(^{7}Be, ^{210}Pb)$ away from Alaska along GP15 and from South America during GP16. The offshore portion of GP16 generally has values of $f(^{7}Be, ^{210}Pb)$ comparable to those of Equatorial/South Pacific samples during

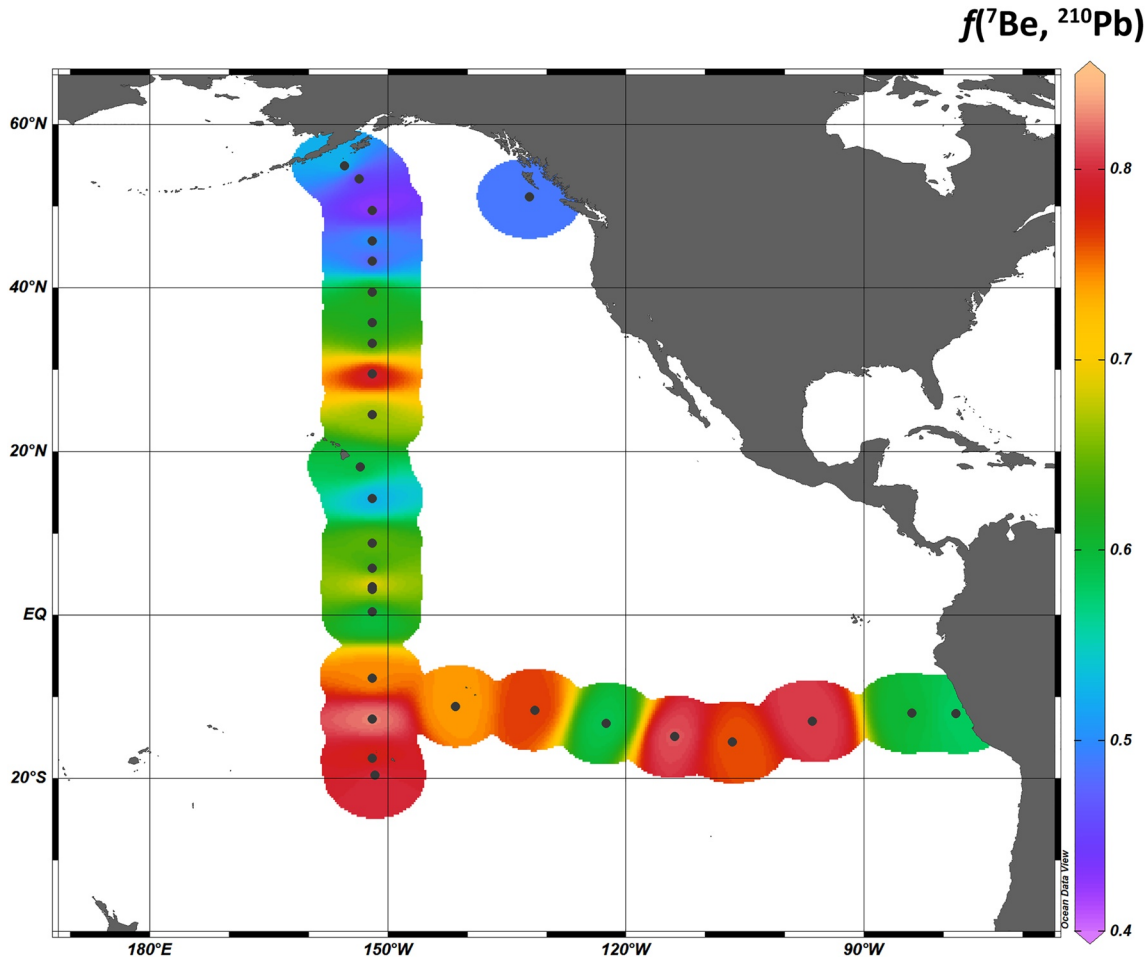

Figure 9. $f(^{7}Be, ^{210}Pb)$ along the GP15 (152°W) and GP16 (12°S) transects.

GP15 (Figure 9; Tables 2 and 3). All but one sample in this region have $f(^{7}Be, ^{210}Pb)$ values above or equal to the marine mean, reaching as high as 0.82. Aerosols with $f(^{7}Be, ^{210}Pb)$ in this range were considered to have an upper troposphere/lower stratosphere provenance by Graustein and Turekian (1996).

3.3.3. Links Between $f(^{7}Be, ^{210}Pb)$ and Trace Elements

Trace element concentrations (Al, Ti, V, Cr, Mn, Fe, Co, Ni, Cu, Zn, Pb) were measured on aerosol samples collected during the GP15 transect (Marsay et al., 2021). On GP16, concentrations of a smaller suite of aerosol trace elements (Al, Ti, V, Mn, Fe, Cu, Cd, Pb) were reported (Buck et al., 2019). Here, we highlight patterns of Al, Ti, Fe, Pb, Co, and Zn on GP15 and Al, Ti, and Fe on GP16 relative to $f(^{7}Be,^{210}Pb)$. (On GP16, the Pb and Co data sets are incomplete due to loading often less than instrumental detection limits and are excluded. The filters used on GP16 were found to have unacceptably high blank concentrations for Zn.) Of the elements considered, Al and Ti are thought to be tracers of crustal (lithogenic) material. Figures 10 and 11 show the trends of the selected trace elements and $f(^{7}Be, ^{210}Pb)$ along the GP15 and GP16 transects, respectively. For GP15, Al, Ti, Fe, Pb, and Co show highest concentrations in the North Pacific (Figure 10). Values generally decrease south of 35°N, although Al and Pb shows maxima at ~10°N. The values of $f(^{7}Be, ^{210}Pb)$ show the inverse trend with low values coincident with high trace element loading. Along the transect, the peaks of $f(^{7}Be, ^{210}Pb)$ generally correspond to low concentrations of lithogenic trace elements such as Al and Ti (Figure 10). In the North Pacific, the section of GP15 closest to continental land masses, the highest Al and Ti concentrations have the lowest $f(^{7}Be, ^{210}Pb)$ values, consistent with a lower troposphere source of the aerosols. Conversely, in the South/Equatorial Pacific, the $f(^{7}Be, ^{210}Pb)$ is equal to or greater than the global marine $f(^{7}Be, ^{210}Pb)$ mean and has low aerosol Al and Ti loading, consistent with an upper troposphere source of aerosols. A notable exception to this pattern is the Al

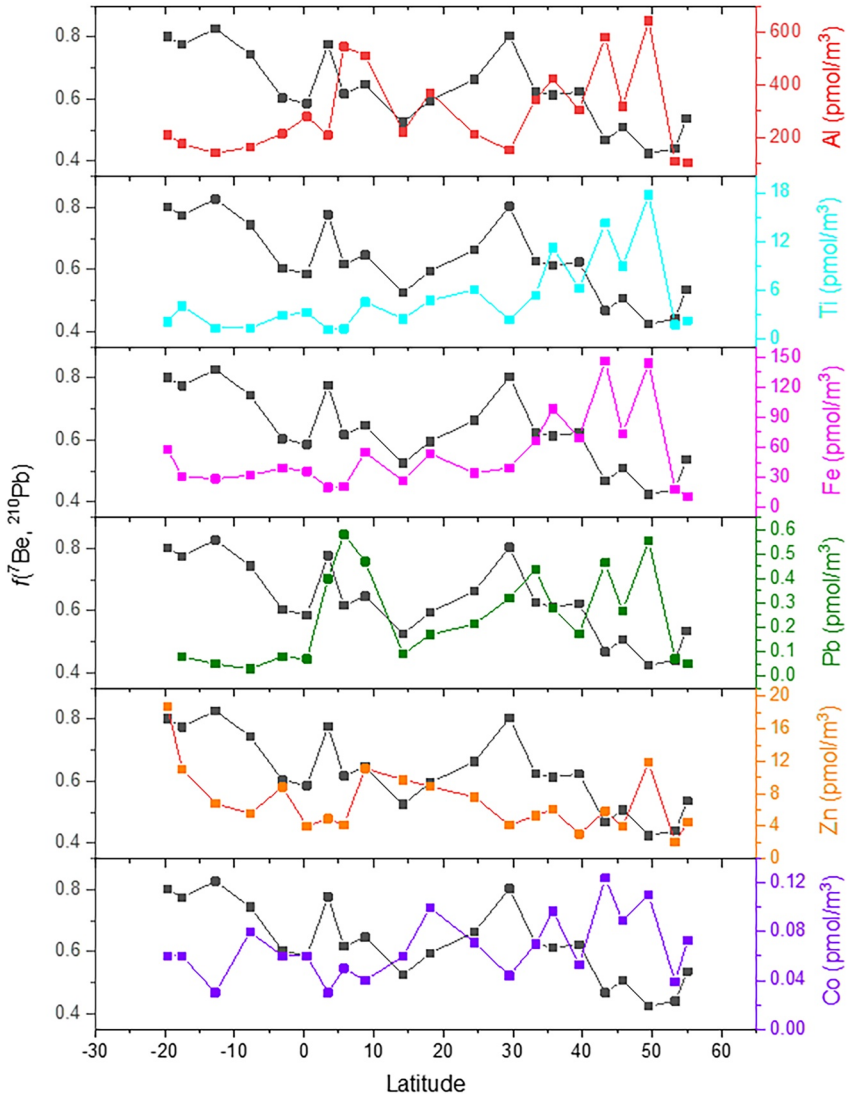

Figure 10. Aerosol trace element concentrations and $f(^{7}Be, ^{210}Pb)$ along the GP15 transect (152°W). Positive latitudes are north.

and $f(^{7}Be, ^{210}Pb)$ values at ~5°N on GP15 (Figure 10) and Al, Ti, and Fe at 120°W on GP16 (Figure 11). Lead shows a weaker relationship with $f(^{7}Be, ^{210}Pb)$, although data from both transects show that away from continental influence, aerosol concentration is low, and aerosols in the marine boundary layer are primarily sourced from the upper troposphere.

Cross plots of the individual trace element concentrations with $f(^{7}Be,^{210}Pb)$ (Figures 12 and 13) emphasize these relationships. Best-fit lines were calculated using a bivariate fit (Cantrell, 2008). For GP15, the correlations with Al ($r = 0.533$), Ti ($r = 0.595$), and Co ($r = 0.537$), and to a lesser extent Fe ($r = 0.502$), show decreasing $f(^{7}Be, ^{210}Pb)$ with increasing elemental concentration, consistent with a lower troposphere source. Pb and Zn show no clear relationship (P-values > 0.05) with $f(^{7}Be,^{210}Pb)$, supporting the input of these trace elements from both lower and upper troposphere sources. On GP16, $f(^{7}Be, ^{210}Pb)$ shows similar relationships with Ti ($r = 0.724$) and Fe ($r = 0.715$), and Al ($r = 0.715$), with stronger correlations than GP15.

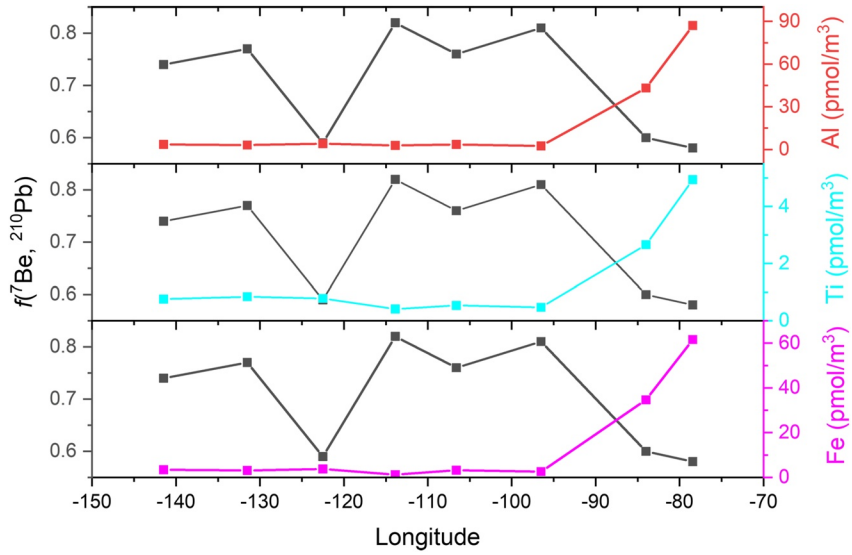

Figure 11. Aerosol trace element concentrations and $f(^{7}Be, ^{210}Pb)$ along the GP16 transect (12°S). Negative longitudes are west.

3.4. Aerosol Sources and $^{210}Po/^{210}Pb$ Ratios Along the GP15 Transect

The $^{210}Po/^{210}Pb$ activity ratio of aerosols primarily reflects the residence time of the aerosols in the atmosphere. Following its production from ^{222}Rn gas in the atmosphere, ^{210}Pb decays via the short-lived ^{210}Bi (half-life = 5 days) to ^{210}Po. As ^{210}Pb is quickly scavenged onto aerosols following its production, the relationships among the three radionuclides can be effectively used to determine mean aerosol residence times (Baskaran, 2011; Burton & Stewart, 1960; Peirson et al., 1966; Semertzidou et al., 2016; Turekian et al., 1977). Aerosol residence times are typically days to weeks (Baskaran, 2011; Carvalho, 1995; H. E. Moore et al., 1973; Turekian et al., 1974), suggesting that the $^{210}Bi/^{210}Pb$ activity ratio is expected to be near the equilibrium value of 1, but the $^{210}Po/^{210}Pb$ ratio will be relatively low, <0.2 (Baskaran, 2011).

Persson and Holm (2014) compiled measurements of the $^{210}Po/^{210}Pb$ ratio in aerosols from the Arctic to Antarctic and noted that the values averaged ~0.25 in the mid-latitudes. Most of the values determined on the GP15 samples are <0.2 within uncertainties. However, there are four samples with $^{210}Po/^{210}Pb$ ratios that exceed 0.2: Aer3, Aer8, Aer11, and Aer21 (Table 1; Figure 4); two, Aer11 and Aer21, have high $f(^{7}Be, ^{210}Pb)$, 0.80 and 0.83, respectively (Table 2), suggesting that the upper troposphere aerosols that comprise them had relatively long residence times before they entered the marine boundary layer (Poet et al., 1972; Tokieda et al., 1996; Tsunogai & Fukuda, 1974). The values of $f(^{7}Be, ^{210}Pb)$ are lower for the Aer3 (0.54) and Aer8 (0.62) samples, and the $^{210}Po/^{210}Pb$ ratio in Aer8 is 0.88 ± 0.32, possibly suggesting that it has a significant component of dust that has ^{210}Po and ^{210}Pb essentially at equilibrium ($^{210}Po/^{210}Pb \sim 1.0$). Yet, neither sample has particularly high concentration of aerosol Al or Ti compared with other high Al and Ti samples that have low $^{210}Po/^{210}Pb$ ratios. Moreover, GP15 samples were taken during a time of year in which dust inputs were typically low (Marsay et al., 2021). Thus, dust may be eliminated as a cause of the anomalously high $^{210}Po/^{210}Pb$ for this sample.

The biogeochemical cycling of ^{210}Po in the surface ocean and volatilization may play a role in the observed aerosol $^{210}Po/^{210}Pb$ ratios. ^{210}Po is typically deficient with respect to radioactive equilibrium with its grandparent ^{210}Pb in surface water. This deficiency may partly be due to is its assimilation into cells as an analog of sulfur (Cherrier et al., 1995; Fisher et al., 1983; Harada et al., 1989; Stewart & Fisher, 2003a). Stewart and Fisher (2003b) showed that Po uptake in marine phytoplankton cultured in the laboratory is explained by both a surface-bound fraction and a cellular fraction associated with protein. Sorption experiments have confirmed that ^{210}Po can be incorporated into proteins (Yang et al., 2015). Such behavior helps account for observed links between chlorophyll α (as a proxy for living organic matter), productivity, POC concentration, and the rates of Po scavenging and regeneration from sinking particles (Choi et al., 2014; Nozaki et al., 1997).

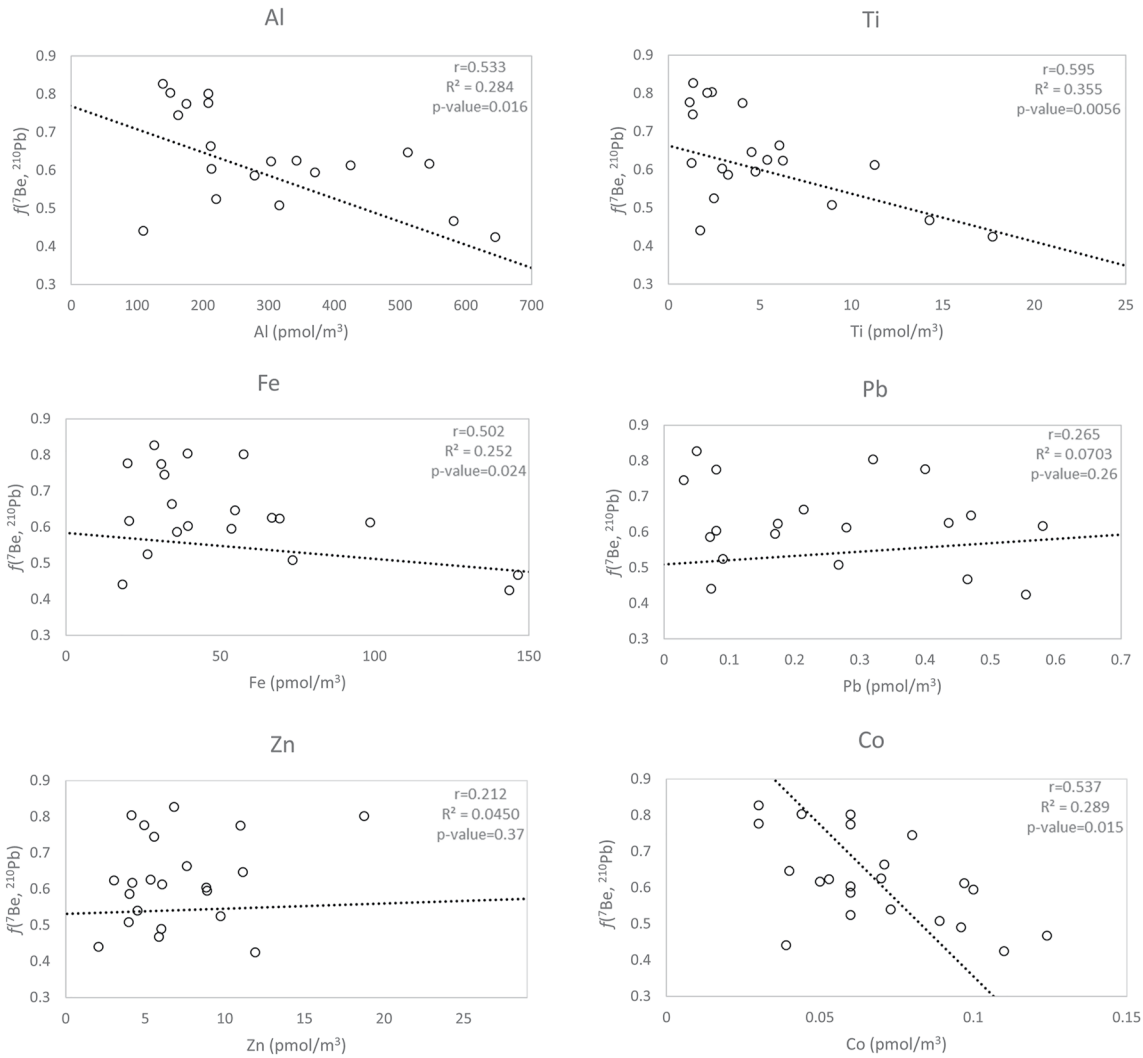

Figure 12. Cross plots of $f(^{7}Be, ^{210}Pb)$ versus trace element concentrations for the GP15 (152°W) transect. Lines are bivariate best fits.

Polonium is classed with the Group 16 metalloids such as selenium and tellurium and may share biogeochemical behavior with them. Dissolved Se in seawater is found as selenite (+IV), selenate (+VI), and dissolved organic selenides (-II), with the latter being the predominant form in surface waters (Cherrier et al., 1995). Tellurium is the closest neighbor to polonium in the periodic table, and Lee and Edmond (1985) argued that the geochemical behavior of tellurium is more similar to that of polonium, showing scavenging as the dominant +VI form (e.g., $Te(OH)_6$) rather than existing as an oxyanion as Se does. However, Lee and Edmond (1985) noted subsurface maxima in Te profiles, suggesting regeneration from particles. Several authors have hypothesized that Po could exist in surface waters as dimethyl polonide (DMPo), similar to dimethyl sulfide (DMS) (Bahrou et al., 2012; Hussain et al., 1995; Kim et al., 2000). In addition, Chuang et al. (2013) found that both organic biopolymers (hydroxamate siderophores) and manganese and iron oxides played a role in binding polonium. Lin et al. (2021) assessed the relative binding affinity of Po in seawater to specific phytoplankton-related biopolymers (e.g., those associated with diatoms vs. coccolithophores). However, the relationship between the volatile pool of Po (e.g., DMPo) and phytoplankton/bacteria remains poorly constrained (Bahrou et al., 2012; Stewart & Fisher, 2003b).

If Po exists as DMPo, it may contribute to the aerosol burden in the marine boundary layer, much like DMS has been shown to do. This would add $^{210}Po > ^{210}Pb$ to aerosols through volatilization or ejection of a colloidal phase from the surface ocean. Turekian et al. (1974) hypothesized that aerosol enrichments of ^{210}Po could occur in the open ocean if plankton-rich particles became part of the aerosol burden. Indeed, enrichment of ^{210}Po relative to ^{210}Pb in the sea surface microlayer was subsequently demonstrated by Bacon and Elzerman (1980), primarily

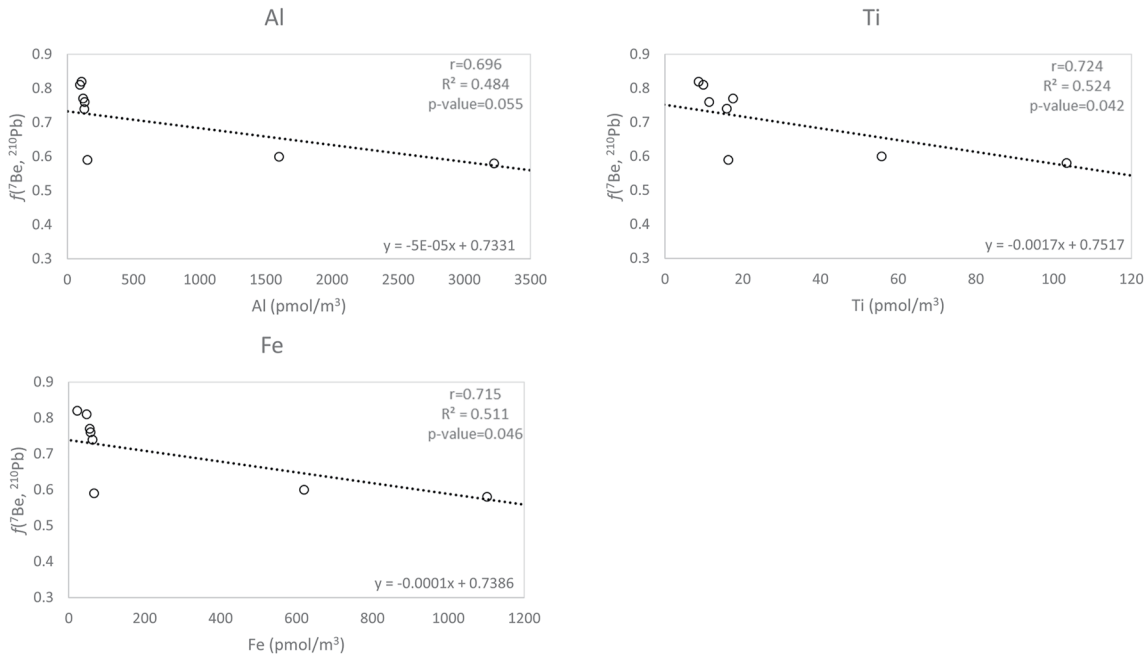

Figure 13. Cross plots of $f(^{7}Be, ^{210}Pb)$ versus trace element concentrations for the GP16 (12°S) transect. Lines are bivariate best fits.

in coastal environments. Bulk surface water along the GP15 transect has $^{210}Po/^{210}Pb$ generally <0.5 (Cochran, unpublished data), so simple sea salt aerosols comprising bulk seawater cannot explain high $^{210}Po/^{210}Pb$. Thus, enrichment of ^{210}Po via a mechanism such as DMPo production and volatilization seems needed to explain high aerosol $^{210}Po/^{210}Pb$. A potential future step into investigating this possibility is to take samples for simultaneous measurement of concentrations of sulfur dimethyl compounds (e.g., DMS) and to measure ^{210}Po and ^{210}Pb on the same samples. Stable sulfur isotopes, which fractionate differently for biotic processes relative to abiotic processes (Calhoun et al., 1991), have provided evidence of biotic DMS production on a molecular level (Amrani et al., 2013; Oduro et al., 2012). Using this method, biotic DMS production has been confirmed in the North and subtropical Pacific (Amrani et al., 2013; Calhoun et al., 1991). Hence, similar biotic processes can be expected to be responsible for the excess ^{210}Po seen in the GP15 samples from the area. The compilation by Persson and Holm (2014) mentioned above found that $^{210}Po/^{210}Pb$ in aerosols collected near the poles had a huge spread, with values as high as 1.6. Recently, sulfur isotope anomalies indicating DMS production have been found in Antarctic Sea ice as a result of metabolism in sea ice algae (Carnat et al., 2018). If DMPo is produced in the same manner, it could help explain anomalously high $^{210}Po/^{210}Pb$ ratios in high-latitude environments.

The Pacific Ocean has been the site for several DMS studies (Andreae & Raemdonck, 1983; Gray et al., 2011; Kieber et al., 1996). Its diverse phytoplankton/bacteria community was demonstrated to contribute to DMS to a great extent through biodegradation of its precursor dimethylsulfoniopropionate (DMSP; Karsten et al., 1996; Keller et al., 1989). Coccolithophores are considered the main contributor of biotic DMSP and its global distribution in surface water has been recently studied by McParland and Levine (2019). Areas in the Pacific high in predicted DMSP emission in the summer and fall overlap with sites of elevated $^{210}Po/^{210}Pb$ at 40°N (Aer8) and near the equator (12.75°S; Aer21). This supports a potential link between DMS and DMPo. It can also serve as a guide for selecting future sampling locations for a combined study of the relationships among DMSP, DMS, and DMPo. Clearly, further research is needed on ^{210}Po cycling in the surface ocean and possible enrichment of this radionuclide in aerosols in high-productivity marine environments.

4. Summary and Conclusions

Aerosol measurements of ^{210}Pb made as part of two GEOTRACES cruises (GP15 and GP16) in the Pacific Ocean, coupled with ^{7}Be-derived bulk deposition velocities, are used to determine ^{210}Pb fluxes at oceanic sites. The ^{7}Be-derived ^{210}Pb fluxes based on short-term aerosol collections in 2018 (GP15) agree well with longer-term

fluxes determined by collection of precipitation at island sites during the SEAREX program in the 1970–1980s. In addition, the ^{7}Be/^{210}Pb activity ratio in aerosols expressed as a normalized fraction of ^{7}Be to ^{210}Pb, $f(^{7}\text{Be}, ^{210}\text{Pb})$, is an effective tracer of aerosol source. With a robust data set, $f(^{7}\text{Be}, ^{210}\text{Pb})$ can serve as a viable independent tracer of aerosol provenance. High values of $f(^{7}\text{Be}, ^{210}\text{Pb})$ indicate an upper troposphere source of aerosols and low values are representative of a continental boundary layer source.

Along the two transects sampled, $f(^{7}\text{Be}, ^{210}\text{Pb})$ increases from values more typical of continental boundary layer sources near the continents to values indicating supply of aerosols from upper troposphere sources to the marine boundary layer at open ocean sites. Values of $f(^{7}\text{Be}, ^{210}\text{Pb})$ show negative correlations with aerosol Al, Ti, and Fe concentrations during both GP15 and GP16, reinforcing the continental source for these trace elements. The relationship with Pb on GP15 shows a very weak correlation with $f(^{7}\text{Be}, ^{210}\text{Pb})$, suggesting that it has a mixed upper-lower troposphere source to the GP15 study region.

The normalized fraction is also helpful in explaining anomalously high ^{210}Po/^{210}Pb ratios in aerosols. Most of the samples collected on GP15 have low ^{210}Po/^{210}Pb (<0.2) indicating relatively short aerosol residence times. Four samples have high ^{210}Po/^{210}Pb. In two of these, $f(^{7}\text{Be}, ^{210}\text{Pb})$ indicates an upper troposphere source and thus potentially longer aerosol residence times. In two others, the values of $f(^{7}\text{Be}, ^{210}\text{Pb})$ suggest a lower troposphere source, but low Al and Ti concentrations imply that dust is not a factor. Instead, we suggest that enrichments of ^{210}Po in the sea surface microlayer as an organic Po species or possibly as volatile dimethyl polonide (DMPo) may be the source.

Data Availability Statement

New data included in this manuscript are given in Tables 1–3 and have been submitted to the Biological and Chemical Oceanography Data Management Office (BCO-DMO). Links to GP15 ^{7}Be and trace element data are https://www.bco-dmo.org/dataset/781794 (Leg 1), and https://www.bco-596.dmo.org/dataset/781806 (Leg 2); for GP16, trace elements: https://www.bco-dmo.org/dataset/675632, for ^{7}Be: https://www.bco-dmo.org/dataset/671814, and for ^{210}Pb: https://www.bco-dmo.org/dataset/675403.

Acknowledgments
Our coauthor David Kadko passed away during the final stages of preparing this manuscript for submission. He was a valued colleague and will be deeply missed. We dedicate this contribution in his memory. This research was supported by National Science Foundation grants OCE-1736591 to J. Kirk Cochran, OCE-1454368 to Clifton S. Buck and William M. Landing, OCE-1756103 to Clifton S. Buck, OCE-123279, OCE-1736319, and OCE-1736612 to David Kadko, and OCE-1756104 to William M. Landing. We thank the captain and crew of the R/V Roger Revelle during GEOTRACES GP15 and Chief Scientists Phoebe Lam, Karen Casciotti, and Greg Cutter for their support. We also thank Drs. Robert Aller and Steven Beaupré for their very useful comments that have improved the manuscript.

References

Amrani, A., Said-Ahmad, W., Shaked, Y., & Kiene, R. P. (2013). Sulfur isotope homogeneity of oceanic DMSP and DMS. *Proceedings of the National Academy of Sciences*, *110*(46), 18413–18418. https://doi.org/10.1073/pnas.1312956110

Andreae, M. O., & Raemdonck, H. (1983). Dimethyl sulfide in the surface ocean and the marine atmosphere: A global view. *Science*, *221*(4612), 744–747. https://doi.org/10.1126/science.221.4612.744

Andrews, J. E., Hartin, C., Buesseler, K. O., & K., O. (2008). ^{7}Be analyses in seawater by low background gamma-spectroscopy. *Journal of Radioanalytical and Nuclear Chemistry*, *277*(1), 253–259. https://doi.org/10.1007/s10967-008-0739-y

Bacon, M. P., & Elzerman, A. W. (1980). Enrichment of ^{210}Pb and ^{210}Po in the sea-surface microlayer. *Nature*, *284*(5754), 332–334. https://doi.org/10.1038/284332a0

Bahrou, A. S., Ollivier, P. R., Hanson, T. E., Tessier, E., Amouroux, D., & Church, T. M. (2012). Volatile dimethyl polonium produced by aerobic marine microorganisms. *Environmental Science & Technology*, *46*(20), 11402–11407. https://doi.org/10.1021/es3006546

Baskaran, M. (2011). Po-210 and Pb-210 as atmospheric tracers and global atmospheric Pb-210 fallout: A review. *Journal of Environmental Radioactivity*, *102*(5), 500–513. https://doi.org/10.1016/j.jenvrad.2010.10.007

Baskaran, M., Coleman, C. H., & Santschi, P. H. (1993). Atmospheric depositional fluxes of ^{7}Be and ^{210}Pb at Galveston and College Station, Texas. *Journal of Geophysical Research*, *98*(D11), 20555–20571. https://doi.org/10.1029/93jd02182

Benninger, L. K., Lewis, D. M., & Turekian, K. K. (1975). The use of natural Pb-210 as a heavy metal tracer in the river—Estuarine system. In *Marine chemistry in the coastal environment*, *ACS symposium series* (Vol. *18*, pp. 202–210).

Bloom, N., & Crecelius, E. A. (1983). Solubility behavior of atmospheric ^{7}Be in the marine environment. *Marine Chemistry*, *12*(4), 323–331. https://doi.org/10.1016/0304-4203(83)90059-2

Buck, C. S., Aguilar-Islas, A., Marsay, C., Kadko, D., & Landing, W. M. (2019). Trace element concentrations, elemental ratios, and enrichment factors observed in aerosol samples collected during the US GEOTRACES eastern Pacific Ocean transect (GP16). *Chemical Geology*, *511*, 212–224. https://doi.org/10.1016/j.chemgeo.2019.01.002

Burton, W. M., & Stewart, N. G. (1960). Use of long-lived natural radioactivity as an atmospheric tracer. *Nature*, *186*(4725), 584–589. https://doi.org/10.1038/186584a0

Calhoun, J. A., Bates, T. S., & Charlson, R. J. (1991). Sulfur isotope measurements of submicrometer sulfate aerosol particles over the Pacific Ocean. *Geophysical Research Letters*, *18*(10), 1877–1880. https://doi.org/10.1029/91gl02304

Cantrell, C. A. (2008). Review of methods for linear least-squares fitting of data and application to atmospheric chemistry problems. *Atmospheric Chemistry and Physics*, *8*(17), 5477–5487. https://doi.org/10.5194/acp-8-5477-2008

Carnat, G., Said-Ahmad, W., Fripiat, F., Wittek, B., Tison, J. L., Uhlig, C., & Amrani, A. (2018). Variability in sulfur isotope composition suggests unique dimethylsulfoniopropionate cycling and microalgae metabolism in Antarctic Sea ice. *Communications biology*, *1*(1), 1–9. https://doi.org/10.1038/s42003-018-0228-y

Carvalho, F. P. (1995). Origins and concentrations of ^{222}Rn, ^{210}Pb, ^{210}Bi and ^{210}Po in the surface air at Lisbon, Portugal, at the Atlantic edge of the European continental landmass. *Atmospheric Environment*, *29*(15), 1809–1819. https://doi.org/10.1016/1352-2310(95)00076-b

Cherrier, J., Burnett, W. C., & LaRock, P. A. (1995). Uptake of polonium and sulfur by bacteria. *Geomicrobiology Journal*, *13*(2), 103–115. https://doi.org/10.1080/01490459509378009

Choi, H. Y., Stewart, G., Lomas, M. W., Kelly, R. P., & Moran, S. B. (2014). Linking the distribution of ^{210}Po and ^{210}Pb with plankton community along line P, Northeast Subarctic Pacific. *Journal of Environmental Radioactivity*, *138*, 390–401. https://doi.org/10.1016/j.jenvrad.2014.02.009

Chuang, C.-Y., Santschi, P. H., Ho, Y.-F., Conte, M. H., Guo, L., Schumann, D., et al. (2013). Role of biopolymers as major carrier phases of Th, Pa, Pb, Po, and Be radionuclides in settling particles from the Atlantic Ocean. *Marine Chemistry*, *157*, 131–143. https://doi.org/10.1016/j.marchem.2013.10.002

Dörr, H., & Münnich, K. O. (1991). Lead and cesium transport in European forest soils. *Water, Air, and Soil Pollution*, *57*(1), 809–818. https://doi.org/10.1007/bf00282944

Fisher, N. S., Burns, K. A., Cherry, R. D., & Heyraud, M. (1983). Accumulation and cellular distribution of ^{241}Am, ^{210}Po and ^{210}Pb in two marine algae. *Marine Ecology Progress Series*, *11*, 233–237. https://doi.org/10.3354/meps011233

Graustein, W. C., & Turekian, K. K. (1986). ^{210}Pb and ^{137}Cs in air and soils measure the rate and vertical profile of aerosol scavenging. *Journal of Geophysical Research*, *91*(D13), 14355. https://doi.org/10.1029/jd091id13p14355

Graustein, W. C., & Turekian, K. K. (1996). ^{7}Be and ^{210}Pb indicate an upper troposphere source for elevated ozone in the summertime subtropical free troposphere of the eastern North Atlantic. *Geophysical Research Letters*, *23*(5), 539–542. https://doi.org/10.1029/96gl00304

Gray, B. A., Wang, Y., Gu, D., Bandy, A., Mauldin, L., Clarke, A., et al. (2011). Sources, transport, and sinks of SO_2 over the equatorial Pacific during the Pacific atmospheric sulfur experiment. *Journal of Atmospheric Chemistry*, *68*(1), 27–53. https://doi.org/10.1007/s10874-010-9177-7

Harada, K., Burnett, W. C., LaRock, P. A., & Cowart, J. B. (1989). Polonium in Florida groundwater and its possible relationship to the sulfur cycle and bacteria. *Geochimica et Cosmochimica Acta*, *53*(1), 143–150. https://doi.org/10.1016/0016-7037(89)90281-0

Hussain, N., Church, T. M., Luther, G. W., III, & Moore, W. S. (1995). ^{210}Po and ^{210}Pb disequilibrium in the hydrothermal vent fluids and chimney deposits from Juan de Fuca Ridge. *Geophysical Research Letters*, *22*(23), 3175–3178. https://doi.org/10.1029/95gl03269

Kadko, D., Aguilar-Islas, A., Buck, C. S., Fitzsimmons, J. N., Landing, W. M., Shiller, A., et al. (2020). Sources, fluxes and residence times of trace elements measured during the US GEOTRACES East Pacific Zonal Transect. *Marine Chemistry*, *222*, 103781. https://doi.org/10.1016/j.marchem.2020.103781

Kadko, D., Landing, W. M., & Buck, C. S. (2020). Quantifying atmospheric trace element deposition over the ocean on a global scale with satellite rainfall products. *Geophysical Research Letters*, *47*(7), e2019GL086357. https://doi.org/10.1029/2019gl086357

Kadko, D., & Olson, D. (1996). Beryllium-7 as a tracer of surface water subduction and mixed-layer history. *Deep Sea Research Part I: Oceanographic Research Papers*, *43*(2), 89–116. https://doi.org/10.1016/0967-0637(96)00011-8

Kadko, D., & Prospero, J. (2011). Deposition of ^{7}Be to Bermuda and the regional ocean: Environmental factors affecting estimates of atmospheric flux to the ocean. *Journal of Geophysical Research*, *116*(C2), C02013. https://doi.org/10.1029/2010JC006629

Karsten, U., Kück, K., Vogt, C., & Kirst, G. O. (1996). Dimethylsulfoniopropionate production in phototrophic organisms and its physiological functions as a cryoprotectant. In *Biological and environmental chemistry of DMSP and related sulfonium compounds* (pp. 143–153). Springer.

Keller, M. D., Bellows, W. K., & Guillard, R. R. (1989). Dimethyl sulfide production in marine phytoplankton.

Kieber, D. J., Jiao, J., Kiene, R. P., & Bates, T. S. (1996). Impact of dimethylsulfide photochemistry on methyl sulfur cycling in the equatorial Pacific Ocean. *Journal of Geophysical Research*, *101*(C2), 3715–3722. https://doi.org/10.1029/95jc03624

Kim, G., Hussain, N., & Church, T. M. (2000). Excess ^{210}Po in the coastal atmosphere. *Tellus B: Chemical and Physical Meteorology*, *36*(1), 65–79. https://doi.org/10.1034/j.1600-0889.2000.00975.x

Koch, D. M., Jacob, D. J., & Graustein, W. C. (1996). Vertical transport of tropospheric aerosols as indicated by ^{7}Be and ^{210}Pb in a chemical tracer model. *Journal of Geophysical Research*, *101*(D13), 18651–18666. https://doi.org/10.1029/96jd01176

Lal, D., & Peters, B. (1967). Cosmic ray produced radioactivity on the Earth. In *Kosmische Strahlung II/cosmic rays II* (pp. 551–612). Springer.

Lambert, G., & Nezami, M. (1965). Importance des retombées séches dans le bilon du plomb-210. *Annales de Geophysique*, *21*, 245–251.

Lee, D. S., & Edmond, J. M. (1985). Tellurium species in seawater. *Nature*, *313*(6005), 782–785. https://doi.org/10.1038/313782a0

Lin, P., Xu, C., Xing, W., & Santschi, P. H. (2021). Molecular Level Characterization of Diatom and Coccolithophore-Associated Biopolymers That Are Binding ^{210}Pb and ^{210}Po in Seawater. *Frontiers in Marine Science*, *8*. https://doi.org/10.3389/fmars.2021.703503

Lozano, R. L., San Miguel, E. G., Bolívar, J. P., & Baskaran, M. (2011). Depositional fluxes and concentrations of ^{7}Be and ^{210}Pb in bulk precipitation and aerosols at the interface of Atlantic and Mediterranean coasts in Spain. *Journal of Geophysical Research*, *116*(18), D18213. https://doi.org/10.1029/2011jd015675

Marsay, C. M., Kadko, D., Landing, W. M., & Buck, C. S. (2021). Bulk aerosol trace element concentrations and deposition fluxes during the US GEOTRACES GP15 Pacific Meridional Transect. *Global Biogeochemical Cycles*, *36*(2), e2021GB007122. In press. https://doi.org/10.1029/2021gb007122

Marsay, C. M., Kadko, D., Landing, W. M., & Buck, C. S. (2022). Bulk aerosol trace element concentrations and deposition fluxes during the US GEOTRACES GP15 Pacific Meridional Transect. *Global Biogeochemical Cycles*, *36*(2), e2021GB007122. https://doi.org/10.1029/2021gb007122

McParland, E. L., & Levine, N. M. (2019). The role of differential DMSP production and community composition in predicting variability of global surface DMSP concentrations. *Limnology & Oceanography*, *64*(2), 757–773. https://doi.org/10.1002/lno.11076

Merrill, J. R., Honda, M., & Arnold, J. R. (1960). Methods for separation and determination of beryllium in sediments and natural waters. *Analytical Chemistry*, *32*(11), 1420–1426. https://doi.org/10.1021/ac60167a014

Monaghan, M. C. (1989). Lead 210 in surface air and soils from California: Implications for the behavior of trace constituents in the planetary boundary layer. *Journal of Geophysical Research*, *94*(D5), 6449–6456. https://doi.org/10.1029/jd094id05p06449

Moore, C. M., Mills, M. M., Arrigo, K. R., Berman-Frank, I., Bopp, L., Boyd, P. W., et al. (2013). Processes and patterns of oceanic nutrient limitation. *Nature Geoscience*, *6*(9), 701–710. https://doi.org/10.1038/ngeo1765

Moore, H. A., & Poet, S. E. (1976). ^{210}Pb fluxes determined from ^{210}Pb and ^{226}Ra soil profiles. *Journal of Geophysical Research*, *81*(6), 1056–1058. https://doi.org/10.1029/jc081i006p01056

Moore, H. E., Poet, S. E., & Martell, E. A. (1973). ^{222}Rn, ^{210}Pb, ^{210}Bi, and ^{210}Po profiles and aerosol residence times versus altitude. *Journal of Geophysical Research*, *78*(30), 7065–7075. https://doi.org/10.1029/jc078i030p07065

Moriizumi, J. U. N., Nagamine, K., Iida, T., & Ikebe, Y. (1996). Estimation of areal flux of atmospheric methane in an urban area of Nagoya, Japan, inferred from atmospheric radon-222 data. *Atmospheric Environment*, *30*(10–11), 1543–1549. https://doi.org/10.1016/1352-2310(95)00481-5

Niedermiller, J., & Baskaran, M. (2019). Comparison of the scavenging intensity, remineralization and residence time of ^{210}Po and ^{210}Pb at key zones (biotic, sediment-water and hydrothermal) along the East Pacific GEOTRACES transect. *Journal of Environmental Radioactivity*, *198*, 165–188. https://doi.org/10.1016/j.jenvrad.2018.12.016

Nozaki, Y., Zhang, J., & Takeda, A. (1997). ^{210}Pb and ^{210}Po in the equatorial Pacific and the Bering sea: The effects of biological productivity and boundary scavenging. *Deep Sea Research Part II: Topical Studies in Oceanography*, *44*(9–10), 2203–2220. https://doi.org/10.1016/s0967-0645(97)00024-6

Obrist, D., Conen, F., Vogt, R., Siegwolf, R., & Alewell, C. (2006). Estimation of Hg^0 exchange between ecosystems and the atmosphere using ^{222}Rn and Hg^0 concentration changes in the stable nocturnal boundary layer. *Atmospheric Environment*, *40*(5), 856–866. https://doi.org/10.1016/j.atmosenv.2005.10.012

Oduro, H., Van Alstyne, K. L., & Farquhar, J. (2012). Sulfur isotope variability of oceanic DMSP generation and its contributions to marine biogenic sulfur emissions. *Proceedings of the National Academy of Sciences*, *109*(23), 9012–9016. https://doi.org/10.1073/pnas.1117691109

Papastefanou, C. (2006). Residence time of tropospheric aerosols in association with radioactive nuclides. *Applied Radiation and Isotopes*, *64*(1), 93–100. https://doi.org/10.1016/j.apradiso.2005.07.006

Pavia, F. J., Anderson, R. F., Winckler, G., & Fleisher, M. Q. (2020). Atmospheric dust inputs, iron cycling, and biogeochemical connections in the South Pacific Ocean from thorium isotopes. *Global Biogeochemical Cycles*, *34*(9), e2020GB006562. https://doi.org/10.1029/2020GB006562

Peirson, D. H., Cambray, R. S., & Spicer, G. S. (1966). Lead-210 and polonium-210 in the atmosphere. *Tellus*, *18*(2), 427–433. https://doi.org/10.3402/tellusa.v18i2-3.9381

Persson, B. R. R., & Holm, E. (2014). ^{7}Be, ^{210}Pb and ^{210}Po in the surface air from the Arctic to Antarctica. *Journal of Environmental Radioactivity*, *138*, 364–374. https://doi.org/10.1016/j.jenvrad.2014.01.008

Piliposian, G. T., & Appleby, P. G. (2003). A simple model of the origin and transport of ^{222}Rn and ^{210}Pb in the atmosphere. *Continuum Mechanics and Thermodynamics*, *15*(5), 503–518. https://doi.org/10.1007/s00161-003-0129-1

Poet, S. E., Moore, H. E., & Martell, E. A. (1972). Lead 210, bismuth 210, and polonium 210 in the atmosphere: Accurate ratio measurement and application to aerosol residence time determination. *Journal of Geophysical Research*, *77*(33), 6515–6527. https://doi.org/10.1029/jc077i033p06515

Rastogi, N., & Sarin, M. M. (2008). Atmospheric ^{210}Pb and ^{7}Be in ambient aerosols over low-and high-altitude sites in semiarid region: Temporal variability and transport processes. *Journal of Geophysical Research*, *113*(D11), D11103. https://doi.org/10.1029/2007JD009298

Renfro, A. A., Cochran, J. K., & Colle, B. A. (2013). Atmospheric fluxes of ^{7}Be and ^{210}Pb on monthly time-scales and during rainfall events at Stony Brook, New York (USA). *Journal of Environmental Radioactivity*, *116*, 114–123. https://doi.org/10.1016/j.jenvrad.2012.09.007

Rigaud, S., Puigcorbé, V., Cámara-Mor, P., Casacuberta, N., Roca-Martí, M., Garcia-Orellana, J., et al. (2013). A methods assessment and recommendations for improving calculations and reducing uncertainties in the determination of ^{210}Po and ^{210}Pb activities in seawater. *Limnology and Oceanography: Methods*, *11*(10), 561–571. https://doi.org/10.4319/lom.2013.11.561

Semertzidou, P., Piliposian, G. T., & Appleby, P. G. (2016). Atmospheric residence time of ^{210}Pb determined from the activity ratios with its daughter radionuclides ^{210}Bi and ^{210}Po. *Journal of Environmental Radioactivity*, *160*, 42–53. https://doi.org/10.1016/j.jenvrad.2016.04.019

Silker, W. B. (1972). Beryllium-7 and fission products in the GEOSECS II water column and applications of their oceanic distributions. *Earth and Planetary Science Letters*, *16*(1), 131–137. https://doi.org/10.1016/0012-821x(72)90247-6

Silker, W. B., Robertson, D. E., Rieck, H. G., Jr., Perkins, R. W., & Prospero, J. M. (1968). Beryllium-7 in ocean water. *Science*, *161*(3844), 879–880. https://doi.org/10.1126/science.161.3844.879

Stewart, G., & Fisher, N. S. (2003a). Bioaccumulation of polonium-210 in marine copepods. *Limnology & Oceanography*, *48*(5), 2011–2019. https://doi.org/10.4319/lo.2003.48.5.2011

Stewart, G., & Fisher, N. S. (2003b). Experimental studies on the accumulation of polonium- 210 by marine phytoplankton. *Limnology & Oceanography*, *48*(3), 1193–1201. https://doi.org/10.4319/lo.2003.48.3.1193

Tagliabue, A., Aumont, O., DeAth, R., Dunne, J. P., Dutkiewicz, S., Galbraith, E., et al. (2016). How well do global ocean biogeochemistry models simulate dissolved iron distributions? *Global Biogeochemical Cycles*, *30*(2), 149–174. https://doi.org/10.1002/2015GB005289

Terzi, L., Wotawa, G., Schoeppner, M., Kalinowski, M., Saey, P. R. J., Steinmann, P., et al. (2020). Radioisotopes demonstrate changes in global atmospheric circulation possibly caused by global warming. *Scientific Reports*, *10*(1). https://doi.org/10.1038/s41598-020-66541-5

Tokieda, T., Yamanaka, K., Harada, K., & Tsunogai, S. (1996). Seasonal variations of residence time and upper atmospheric contribution of aerosols studied with Pb-210, Bi-210, Po-210 and Be-7. *Tellus B: Chemical and Physical Meteorology*, *48*(5), 690–702. https://doi.org/10.1034/j.1600-0889.1996.t01-4-00006.x

Tsunogai, S., & Fukuda, K. (1974). Pb-210, Bi-210, and Po-210 in meteoric precipitation and the residence time of tropospheric aerosol. *Geochemical Journal*, *8*(3), 141–152. https://doi.org/10.2343/geochemj.8.141

Tsunogai, S., Suzuki, T., Kurata, T., & Uematsu, M. (1985). Seasonal and areal variation of continental aerosol in the surface air over the Western North Pacific region. *Journal of the Oceanographical Society of Japan*, *41*(6), 427–434. https://doi.org/10.1007/bf02109036

Turekian, K. K., Benninger, L. K., & Dion, E. P. (1983). ^{7}Be and ^{210}Pb total depositional fluxes at New Haven. Connecticut and at Bermuda. *Journal of Geophysical Research*, *88*(5), 411–415. https://doi.org/10.1029/jc088ic09p05411

Turekian, K. K., & Cochran, J. K. (1981a). ^{210}Pb in surface air at Enewetak and the Asian dust flux to the Pacific. *Nature*, *292*(5823), 522–524. https://doi.org/10.1038/292522a0

Turekian, K. K., & Cochran, J. K. (1981b). ^{210}Pb in surface air at Enewetak and the Asian dust flux to the Pacific: Correction. *Nature*, *294*, 670.

Turekian, K. K., & Graustein, W. C. (2003). Natural radionuclides in the Atmosophere. In R. F. Keeling (Ed.), *Treatise on Geochemistry*. Executive Editors: Heinrich D. Holland and Karl K. Turekian. (Vol. 4, pp. 261–279). Elsevier.

Turekian, K. K., Graustein, W. C., & Cochran, J. K. (1989). Lead-210 in the SEAREX program: An aerosol tracer across the Pacific. *Chemical Oceanography*, *10*, 51–81.

Turekian, K. K., Kharkar, D. P., & Thomson, J. (1974). The fates of Pb 210 and Po 210 in the ocean surface. *Journal de Recherches Atmospheriques*, *8*(3), 639–646.

Turekian, K. K., Nozaki, Y., & Benninger, L. K. (1977). Geochemistry of atmospheric radon and radon products. *Annual Review of Earth and Planetary Sciences*, *5*(1), 227–255. https://doi.org/10.1146/annurev.ea.05.050177.001303

Usoskin, I. G., & Kovaltsov, G. A. (2008). Production of cosmogenic ^{7}Be isotope in the atmosphere: Full 3-D modeling. *Journal of Geophysical Research*, *113*(D12), D12107. https://doi.org/10.1029/2007JD009725

Wei, Z. (2021). *^{210}Pb and ^{7}Be as coupled flux and source tracers for aerosols in the Pacific Ocean. Master's Thesis* (p. 34). Stony Brook University.

Wilkening, M. H., & Clements, W. E. (1975). Radon 222 from the ocean surface. *Journal of Geophysical Research*, *80*(27), 3828–3830. https://doi.org/10.1029/jc080i027p03828

Yang, W., Guo, L., Chuang, C., Santschi, P. H., Schumann, D., & Ayranov, M. (2015). Influence of organic matter on the adsorption of 210Pb, 210Po and 7Be and their fractionation on nanoparticles in seawater. https://doi.org/10.1016/j.epsl.2015.05.007

Young, J. A., & Silker, W. B. (1980). Aerosol deposition velocities on the Pacific and Atlantic Oceans calculated from ^{7}Be measurements. *Earth and Planetary Science Letters*, *50*(1), 92–104. https://doi.org/10.1016/0012-821X(80)90121-1

Zhang, F., Wang, J., Baskaran, M., Zhong, Q., Wang, Y., Paatero, J., & Du, J. (2021). A global dataset of atmospheric ^{7}Be and ^{210}Pb measurements: Annual air concentration and depositional flux. *Earth System Science Data*, *13*(6), 2963–2994. https://doi.org/10.5194/essd-13-2963-2021